

# Interplanetary Scintillation studies with the Murchison Wide-field Array IV: The hosts of sub-arcsecond compact sources at low radio frequencies

Elaine M. Sadler,<sup>1,2,3\*</sup> Rajan Chhetri,<sup>2,4</sup> John Morgan,<sup>4</sup> Elizabeth K. Mahony,<sup>1,2,3</sup>  
Thomas H. Jarrett<sup>5</sup> and Steven Tingay<sup>4</sup>

<sup>1</sup>*Sydney Institute for Astronomy, School of Physics A28, The University of Sydney, NSW 2006, Australia*

<sup>2</sup>*ARC Centre of Excellence for All-Sky Astrophysics (CAASTRO)*

<sup>3</sup>*CSIRO Astronomy and Space Science, PO Box 76, Epping, NSW 1710, Australia*

<sup>4</sup>*International Centre for Radio Astronomy Research, Curtin University, GPO Box U1987, Perth, WA 6845, Australia*

<sup>5</sup>*Department of Astronomy, University of Cape Town, Private Bag X3, Rondebosch, 7701, South Africa*

Accepted XXX. Received YYY; in original form ZZZ

## ABSTRACT

Around 10% of bright low-frequency radio sources observed with the Murchison Wide-field Array (MWA) show strong Interplanetary Scintillation (IPS) on timescales of a few seconds, implying that almost all their low-frequency radio emission comes from a compact component less than 0.5 arcsec in angular size. Most of these objects are compact steep-spectrum (CSS) or MHz-peaked spectrum (MPS) radio sources. We have used mid-infrared data from the Wide-field Infrared Survey Explorer (WISE) catalogue to search for the host galaxies of 65 strongly-scintillating MWA sources and compare their properties with those of the overall population of bright low-frequency radio sources. We identified WISE mid-infrared counterparts for 91% of the bright sources in a single 900 deg<sup>2</sup> MWA field, and found that the hosts of the strongly-scintillating sources were typically at least 1 mag fainter in the WISE W1 (3.4 μm) band than the hosts of weakly-scintillating MWA sources of similar radio flux density. This difference arises mainly because the strongly-scintillating sources are more distant. We estimate that strongly-scintillating MWA sources have a median redshift of  $z \sim 1.5$ , and that at least 30% of them are likely to lie at  $z > 2$ . The recently-developed wide-field IPS technique therefore has the potential to provide a powerful new tool for identifying high-redshift radio galaxies without the need for radio spectral-index selection.

**Key words:** galaxies: active – radio continuum: galaxies – quasars: supermassive black holes

## 1 INTRODUCTION

Morgan et al. (2018b) recently developed a novel technique that uses high time-resolution imaging with the Murchison Widefield Array (MWA; Tingay et al. (2013)) to measure interplanetary scintillation (IPS) for many hundreds of radio sources simultaneously across a wide area of sky. Since strong IPS is only seen for sources that are dominated by a compact component less than  $\sim 0.5$  arcsec in size, this technique makes it possible to identify large numbers of sub-arcsecond radio sources efficiently without the need for VLBI observations.

Chhetri et al. (2018a) applied this technique to a five-

minute observation of a 900 deg<sup>2</sup> MWA field at 162 MHz with 0.5 s time resolution, and found that 12% of the strong continuum sources in this field showed rapid fluctuations caused by IPS. Interestingly, Chhetri et al. (2018a) showed that the compact source population at low frequencies is dominated by peaked-spectrum radio sources, and that many of the flat-spectrum QSOs that are compact at frequencies of a few GHz show extended structure at 160 MHz. All the sources studied by Chhetri et al. (2018a) are also catalogued in the 72–231 MHz MWA GLEAM survey (Wayth et al. 2015; Hurley-Walker et al. 2017).

Our aim in this paper is to identify the host galaxies of the compact low-frequency sources found by Chhetri et al. (2018a), and to compare their properties with those of the host galaxies of other bright MWA sources. Since the

\* E-mail: elaine.sadler@sydney.edu.au (EMS)

Chhetri et al. (2018a) sample contains a significant number of peaked-spectrum radio sources, we can also test the recent suggestion (Coppejans et al. 2015; Callingham et al. 2017) that many MHz peaked-spectrum (MPS) radio sources are high-redshift objects at  $z > 2$ .

We take as a reference point the detailed spectroscopic studies of low-frequency radio sources listed in Table 1. Together, these provide a broad picture of the typical optical hosts (and redshift distribution) of bright (flux density above  $\sim 1$  Jy), low-frequency radio sources.

At flux densities above 5–10 Jy, the 178 MHz-selected sample of Laing et al. (1983) and the 408 MHz-selected sample of Best et al. (1999) each provide samples of  $\sim 200$  well-studied sources. Both studies have an optical identification rate close to 100% and near-complete optical spectroscopic information on the radio-source hosts. Despite the difference in selection frequency, both samples contain a similar mix of 70–75% radio galaxies and 25–30% radio-loud QSOs and have a very similar median redshift ( $z \sim 0.48$ ). It therefore seems reasonable to assume that the overall properties of radio sources selected at  $\sim 150$  MHz should be broadly similar to those of samples selected at 408 MHz.

The 408 MHz MRC-1 Jy survey (McCarthy et al. 1996; Kapahi et al. 1998b; Baker et al. 1999) probes a flux-density range similar to that of the Chhetri et al. (2018a) 162 MHz sample. As can be seen from Table 1, 96% of the sources in the MRC-1 Jy sample have been optically identified. Roughly 80% of the MRC-1 Jy sources are radio galaxies, and 20% are radio-loud QSOs.

## 2 SAMPLE SELECTION AND WISE CROSS-MATCHING

### 2.1 Overview

The data samples analysed in this paper are drawn from the 900 deg<sup>2</sup> MWA field observed by Chhetri et al. (2018a). To identify the host galaxies of these sources, we used the all-sky mid-IR Wide-field Infrared Survey Explorer (WISE) allWISE catalogue (Wright et al. 2010; Cutri et al. 2013). This is currently the deepest large-area photometric catalogue available, and most powerful radio AGN out to redshift  $z \sim 1.5$  are expected to have a counterpart in the WISE catalogue (Gürkan et al. 2014; Glowacki et al. 2017).

The relatively high surface density of WISE sources (up to 10,000 deg<sup>-2</sup> at high Galactic latitude) means that sub-arcsec radio positions are needed for reliable cross-matching. Achieving this can be challenging for extended low-frequency sources, which often have complex radio structures with no prominent central core. We therefore took a two-step approach to cross-matching the Chhetri et al. (2018a) MWA sources.

(i) We first compiled a *main IPS-FIRST sample* of MWA sources from Table 1 of Chhetri et al. (2018a), selected to have high enough S/N that they can be reliably split into scintillation classes. This sample includes many sources with complex or extended radio structure, so we used the VLA FIRST survey as the basis for our WISE cross-matching as described in §2.2 below. Since the FIRST survey overlaps only the northern part of the MWA field, the main sample

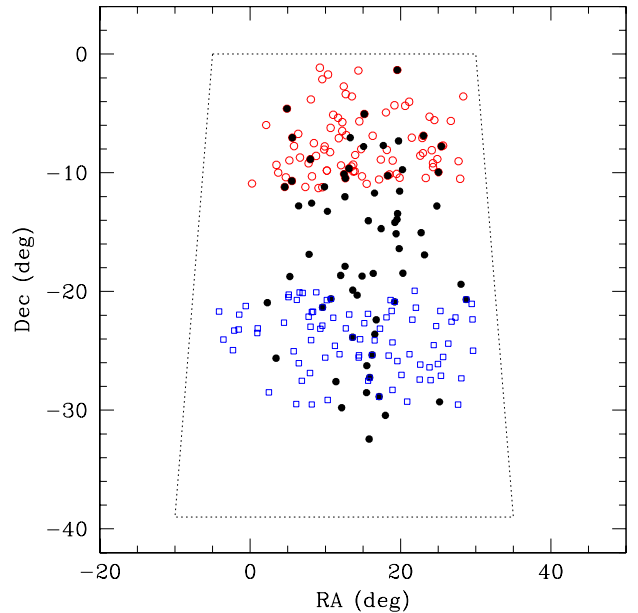


**Figure 1.** Distribution on the sky of the three data samples defined in §2.1. Sources in the *main IPS-FIRST* sample are shown by red open circles, those in the *expanded compact* sample by black filled circles, and those in the *IPS-MRC-1Jy* sample by blue open squares. Dotted lines mark out the full area of the MWA IPS field.

contains only the 88 high S/N sources that lie in this overlap area (see Figure 1).

(ii) We also compiled an *expanded compact* sample of sources that show strong IPS as defined by Chhetri et al. (2018a). These strongly-scintillating sources are known to be compact on sub-arcsec scales at 162 MHz, and experience shows that identifications can be made fairly reliably from the lower-resolution NVSS data. For these compact objects therefore, we can relax both the SNR limit and the restriction that sources need to lie within the FIRST overlap area. The expanded compact sample comprises 65 strongly-scintillating sources, as discussed in §2.3 below.

(iii) In addition, there are 85 Chhetri et al. (2018a) high S/N (normSNR $\geq 12.5$ ) sources in the MRC-1Jy catalogue (McCarthy et al. 1996; Kapahi et al. 1998b), which covers two strips of sky between  $-20^\circ$  and  $-30^\circ$  declination. This *IPS-MRC-1Jy sample* has a different selection frequency from the other two samples (408 MHz rather than 162 MHz), and as a result it is skewed towards slightly brighter sources than the other two sub-samples. It does however contain additional information that will be valuable for later analysis, including accurate radio positions, galaxy/QSO classifications for all sources, and over 40 sources with published spectroscopic redshifts.

The overall properties of these three samples are summarised in Table 2 (where columns 6 and 7 show the number of sources classified as either compact or peaked-spectrum by Chhetri et al. (2018a) and column 8 the number of sources detected in the Australia Telescope 20 GHz (AT20G) survey (Murphy et al. 2010)). Figure 1 shows the sky distribution of the three samples described above.

**Table 1.** Summary of large-area spectroscopic samples of bright low-frequency radio sources. The location of each sample on the sky area is indicated in column 3 as: N = Northern hemisphere, S = Southern hemisphere, E = Equatorial. Our IPS field overlaps with parts of the MRC-BRL, MS4 and MRC-1Jy survey areas.

Sample	Freq. (MHz)	Sky area	Flux density limit (Jy)	Sources	References	Notes	Median redshift
3CR	178	N	10.9	205	Laing et al. (1983)	Optical ID rate 96% (71% galaxies, 25% QSOs)	0.48
MRC-BRL	408	E	5.0	178	Best et al. (1999)	Optical ID rate 100% Spectroscopic completeness 98% (72% galaxies, 28% QSOs)	0.47
MS4	408	S	4.0	228	Burgess & Hunstead (2006a,b)	Optical ID rate > 90%	~0.5
MRC-1 Jy	408	S	0.95	558	McCarthy et al. (1996); Kapahi et al. (1998b) and Baker et al. (1999)	Optical ID rate 96% (80% galaxies, 20% QSOs)	0.63

**Table 2.** Overview of data samples used. All sources are selected from Table 1 of Chhetri et al. (2018a), and compact sources are defined to be those with a normalised scintillation index (NSI)  $\geq 0.9$ , meaning that 90% of the low-frequency flux density arises from a sub-arcsec compact component. The lower S/N cutoff adopted for the expanded compact sample means that this sample contains more faint sources and so has a lower median flux density.

Sample	normSNR	Area	NSI	n	Compact	Peak	AT20G	Median $\alpha_{162}^{1400}$	Notes
Main IPS-FIRST sample	$\geq 12.5$	FIRST overlap area only	All	88	14 (16%)	8 (9%)	20 (23%)	-0.84	$S_{162} \geq 1.08$ Jy (median = 2.28 Jy)
Expanded compact sample	$\geq 8.0$	Full IPS field	$\geq 0.90$	65	65 (100%)	27 (42%)	15 (23%)	-0.67	$S_{162} \geq 0.57$ Jy (median = 1.34 Jy)
IPS-MRC-1 Jy sample	$\geq 12.5$	MRC-1 Jy overlap area	All	85	10 (12%)	7 (8%)	18 (21%)	-0.78	$S_{162} \geq 1.05$ Jy (median = 2.64 Jy)

## 2.2 Radio cross-matching

To derive the most accurate radio positions for WISE cross-matching, we matched the MWA GLEAM sources with objects in the higher-resolution 1.4 GHz FIRST (Becker et al. 1995) and NVSS (Condon et al. 1998) catalogues. This cross-matching process is reasonably straightforward, since the MWA sources are bright enough at 162 MHz that they should be easily detectable in the higher-frequency surveys even if resolved into two or more components.<sup>1</sup>

For the *main IPS-FIRST sample*, we examined the FIRST catalogue and images for all the ‘high S/N’ (norm-SNR  $\geq 12.5$ ) sources from Table 1 of Chhetri et al. (2018a) that lay within the FIRST overlap area. Where two or more FIRST sources lay within the MWA beam, we used well-established criteria (see e.g. section 3.3 of Ching et al. (2017)) to associate double and triple sources and measure a radio centroid. Of the 88 sources in Table 3, 37 have a single FIRST component, 32 are resolved doubles in FIRST and 19 are associated with three or more FIRST components. For

sources matched with a single FIRST component, the median offset between the FIRST and MWA GLEAM positions was 3.2 arcsec.

For the *expanded compact sample*, where all the MWA sources are expected to be single and unresolved on arcsec scales, we carried out a simple cross-match with the NVSS catalogue. All the objects in this sample were reliably matched with a single NVSS source, and for these bright sources the NVSS positional accuracy is typically better than 1.5 arcsec. The median offset between the NVSS and MWA GLEAM positions was 3.4 arcsec.

For the *IPS-MRC-1Jy sample*, we used the radio core positions measured by McCarthy et al. (1996) and Kapahi et al. (1998b), which are typically accurate to better than 1 arcsec.

## 2.3 The main IPS-FIRST sample

We restricted our main sample to the 88 high S/N sources from Chhetri et al. (2018a) that lie within the 1.4 GHz VLA FIRST survey area. This allows us to use the high-resolution FIRST data to characterise the radio structure, and to measure a more accurate radio centroid for sources with extended radio structure. These radio sources are bright enough that most of them can be reliably divided into three

<sup>1</sup> As noted by Chhetri et al. (2018a), the one exception in their sample is the steep-spectrum cluster relic GLEAM J004130-092221 (MRC 0038-096), which is resolved out and undetected in the FIRST survey.

IPS classes on the basis of their normalised scintillation index (NSI), as discussed in §4.1 of [Chhetri et al. \(2018a\)](#) (a few high S/N sources have NSI upper limits between 0.4 and 0.6, and so may be either weak or moderate scintillators).

- 10% are strong scintillators with  $\text{NSI} \geq 0.9$ , in which all the observed flux density arises from a region less than 0.5 arcsec in angular size,
- 27% are moderate scintillators, with  $0.4 \leq \text{NSI} < 0.9$ , where most of the observed flux density arises from one or more sub-arcsec compact components, and
- 63% show weak or no scintillation, with  $\text{NSI} < 0.4$ , and most of the observed flux density is extended on scales of a few arcsec or larger.

Well-developed and reliable techniques already exist for matching FIRST radio data with large optical surveys (e.g. [Best et al. 2005](#); [Ching et al. 2017](#)). In this paper we use the same methodology as [Ching et al. \(2017\)](#), including their technique for associating components of multi-component sources.

For sources with a single FIRST component (42% of the main sample), we used a 2.5 arcsec matching radius to search for a WISE counterpart. For sources with multiple FIRST components, we used the FIRST radio centroid with the same 2.5 arcsec matching radius, and also made a visual inspection of overlay plots like those shown in [Figure 2](#).

We found WISE matches for 80/88 (91%) of sources in the main IPS-FIRST sample. Notes on some individual sources are in the Appendix.

#### 2.4 The expanded compact source sample

An expanded sample of strongly-scintillating sources, also from [Table 1 of Chhetri et al. \(2018a\)](#), was selected to have  $\text{normSNR} \geq 8.0$  and  $\text{NSI} \geq 0.90$ . We were able to relax the S/N cut for these compact sources, since the high level of scintillation they show can be reliably detected even for weaker sources. The final ‘expanded compact’ sample contains 65 objects, of which 18 are also in the main IPS-FIRST sample and a further eight are in the IPS-MRC-1Jy sample.

Not all the sources in the expanded compact sample lie in the FIRST overlap area, but the compact nature of these sources means that we can use the radio positions from the lower-resolution NVSS survey to match with WISE (again using a 2.5 arcsec matching radius).

This initial comparison found WISE matches for 53/65 (82%) of sources in the main sample. For objects with no catalogued WISE source within 2.5 arcsec of the radio position, one of us (THJ) inspected WISE images of the region around the radio-source position to: (i) search for any fainter, uncatalogued WISE sources, and (ii) check for any objects with AGN-like WISE colours ( $W1-W2 > 0.60$  mag) with offsets slightly larger than 2.5 arcsec. This process identified six further WISE counterparts, three of which were significantly fainter in  $W1$  than the allWISE catalogue limit, giving a final WISE identification rate of 59/65 (91%).

#### 2.5 The IPS-MRC-1Jy sample

The [Chhetri et al. \(2018a\)](#) IPS field overlaps part of the MRC-1Jy catalogue area at  $-20^\circ$  to  $-30^\circ$  declination. There

are 85 high S/N ( $\text{normSNR} \geq 12.5$ ) sources from the [Chhetri et al. \(2018a\)](#) catalogue that are also in the MRC-1Jy radio galaxy ([McCarthy et al. 1996](#)) or QSO ([Kapahi et al. 1998b](#)) catalogue, and the accurate radio positions available for the MRC-1Jy sources ([Kapahi et al. 1998a](#)) allow us to make reliable cross-matches with the WISE catalogue. We found WISE matches for 81/85 (95%) of the MRC-1Jy subsample.

#### 2.6 Data tables

Tables [3](#), [4](#) and [5](#) provide information for the main IPS-FIRST sample, the expanded compact source sample and the IPS-MRC-1Jy sample respectively.

The redshift references in [Tables 3](#) (column 15), [4](#) (column 13) and [5](#) (column 14) are coded as follows:

6dFGS:	6dF Galaxy Survey ( <a href="#">Jones et al. 2009</a> )
Ba99:	<a href="#">Baker et al. (1999)</a>
Du89:	<a href="#">Dunlop et al. (1989)</a>
Dr03:	<a href="#">Drake et al. (2003)</a>
Ho03:	<a href="#">Hook et al. (2003)</a>
Ka98:	<a href="#">Kapahi et al. (1998b)</a>
Mc91:	<a href="#">McCarthy et al. (1991)</a>
Mc96:	<a href="#">McCarthy et al. (1996)</a>
Os94:	<a href="#">Osmer et al. (1994)</a>
RC3:	Third Reference Catalogue of Bright Galaxies ( <a href="#">de Vaucouleurs et al. 1991</a> )
Sc65:	<a href="#">Schmidt (1965)</a>
SDSS:	Sloan Digital Sky Survey DR14 ( <a href="#">Abolfathi et al. 2018</a> )
Ti11:	<a href="#">Titov et al. (2011)</a>
We99:	<a href="#">Wegner et al. (1999)</a>
Wi76:	<a href="#">Wills &amp; Wills (1976)</a>
Wo00:	<a href="#">Wold et al. (2000)</a>
Wr83:	<a href="#">Wright et al. (1983)</a>

### 3 RESULTS

#### 3.1 Mid-IR properties of sources in the IPS field

##### 3.1.1 Overall mid-IR properties

The WISE two-colour diagrams shown in [Figures 3](#) and [4](#) provide a first look at the mid-IR properties of bright low-frequency radio sources out to redshift  $z \sim 1$  and beyond.

[Jarrett et al. \(2017\)](#) have shown that WISE colors can provide useful insights into extragalactic radio sources and their evolutionary state. Normal galaxies where the mid-IR emission is dominated by starlight typically have  $W1-W2 < 0.6$  mag ([Wright et al. 2010](#)), with early-type galaxies generally having low  $W2-W3$  colours ( $W2-W3 < 1.5$ ) and star-forming galaxies higher values ( $W2-W3 > 1.0$ ). Very dusty star-forming galaxies and ULIRGs typically have  $W2-W3 > 4$ . QSOs and other powerful ‘radiative-mode’ AGN have  $W1-W2 > 0.8$ , implying that light from the AGN dominates the mid-IR SED.

As can be seen from [Figure 3](#), the radio-loud QSOs detected at 162 MHz span a fairly narrow range in WISE two-colour space, and mainly lie near the WISE ‘blazar strip’

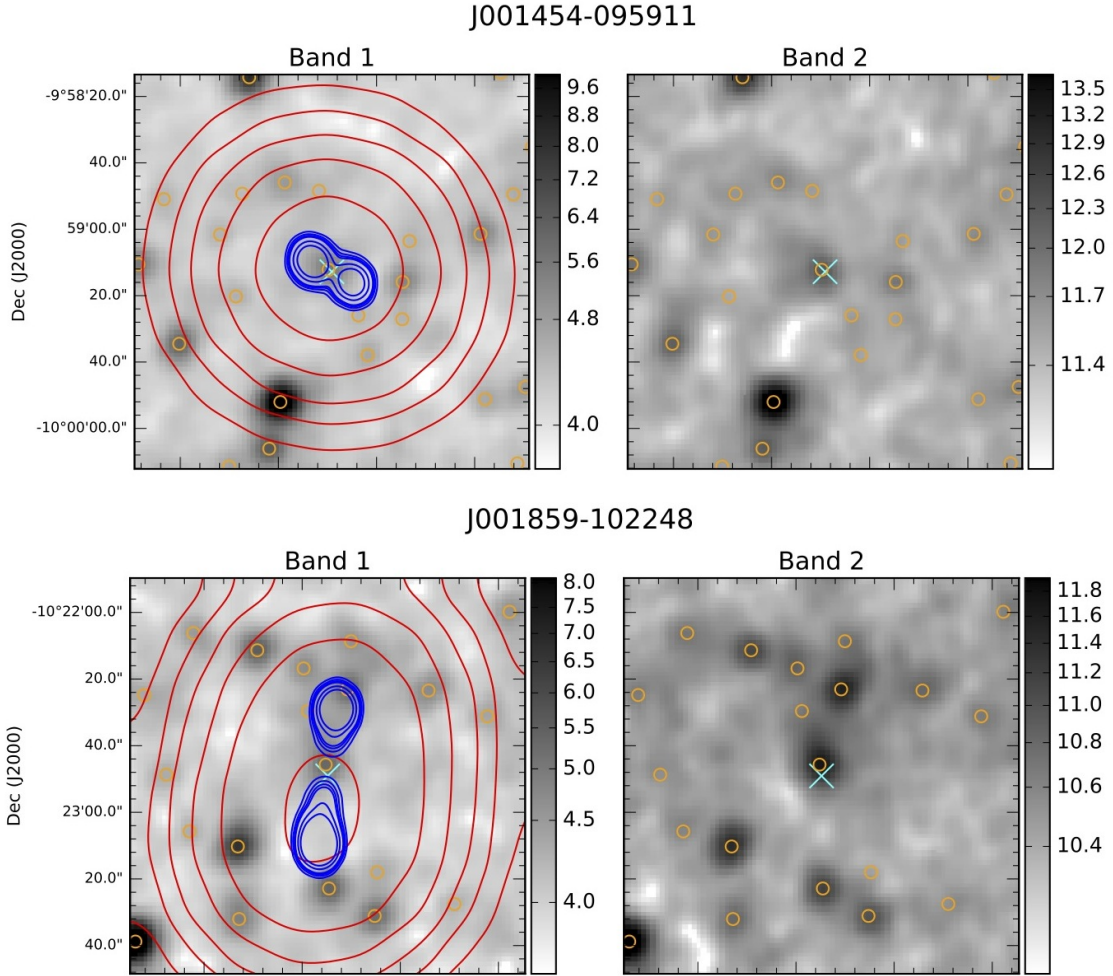


**Figure 2.** Examples of the overlay plots used to assist identification of MWA sources. Greyscale images show the WISE W1 ( $3.4\mu\text{m}$ ) and W2 ( $4.6\mu\text{m}$ ) data, with radio contours overlaid on the W1 image. Red contours correspond to the 162 MHz MWA data and blue contours to the higher-resolution VLA FIRST data. A cyan cross marks the FIRST radio centroid, and orange circles mark mid-IR sources listed in the AllWISE catalogue (Cutri et al. 2013). For both MWA sources shown here, the WISE source closest to the radio centroid was accepted as a genuine ID.

defined by Massaro et al. (2012). In contrast, the radio galaxies show a large spread across the two-colour diagram, and include both objects with colours typical of galaxies and objects with QSO-like mid-IR colours.

Figure 4 shows a WISE two-colour plot split by scintillation class. Most of the strongly-scintillating and moderately-scintillating sources lie in the region with  $W1-W2 > 0.8$  mag where the AGN light outshines the host galaxy, implying that most of these objects are radiatively-efficient AGN (high-excitation radio galaxies and QSOs; see e.g. Heckman & Best (2014)). In contrast, over half of the more extended radio sources with weak or no scintillation have  $W1-W2 < 0.8$  mag, implying that they are radiatively inefficient (low-excitation, or ‘jet-mode’) AGN whose mid-IR emission is dominated by stellar light from the host galaxy (Ching et al. 2017).

At this stage, the main conclusion that can be drawn from Figures 3 and 4 is that most of the strongly-scintillating IPS sources appear to be high-excitation radio galaxies (HERGs; Heckman & Best (2014)) or radio-loud QSOs.

### 3.1.2 The main IPS-FIRST sample

Of the 88 main-sample sources in the FIRST overlap area (Table 3), 80 (91%) are reliably matched with a catalogued WISE source but only 29 (33%) have a known redshift. The mid-IR properties of these radio sources should be typical of the overall MWA source population at flux densities near  $\sim 1$  Jy.

Of the 80 sources with WISE IDs, 37 (46%) have  $W1-W2$  colours  $> 0.8$ , i.e. consistent with a radiatively-efficient AGN, and 43 (54%) have  $W1-W2$  colours  $\leq 0.8$ , i.e. dominated by galaxy stellar light. Thus the main sample contains a roughly equal mixture of ‘radiative mode’ and ‘jet mode’ radio AGN (Heckman & Best 2014).

Table 6 compares the WISE properties of main-sample sources in the three scintillation classes defined by Chhetri et al. (2018a). As can also be seen from Figure 5, the compact sources with  $NSI \geq 0.9$  are typically significantly fainter in W1 than the extended sources with  $NSI < 0.9$ . There are at least two plausible reasons for this - (i) the compact sources could be on average more distant than the extended sources,

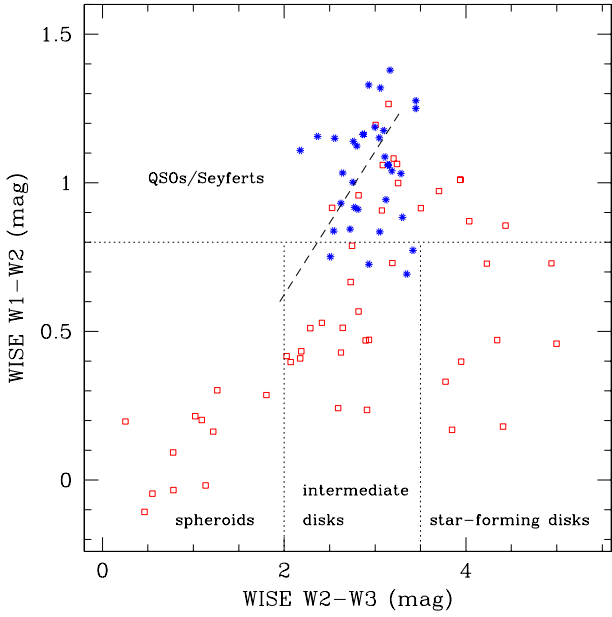


**Figure 3.** A WISE two-colour diagram (Wright et al. 2010) for objects in Tables 3, 4 and 5 that have reliable detections in all three WISE bands W1 ( $3.4\mu\text{m}$ ), W2 ( $4.6\mu\text{m}$ ) and W3 ( $12\mu\text{m}$ ). Blue points show QSOs, and galaxies are shown by open red squares. The diagonal dashed line marks the ‘WISE blazar strip’ occupied by blazars and radio-loud QSOs (Massaro et al. 2012).

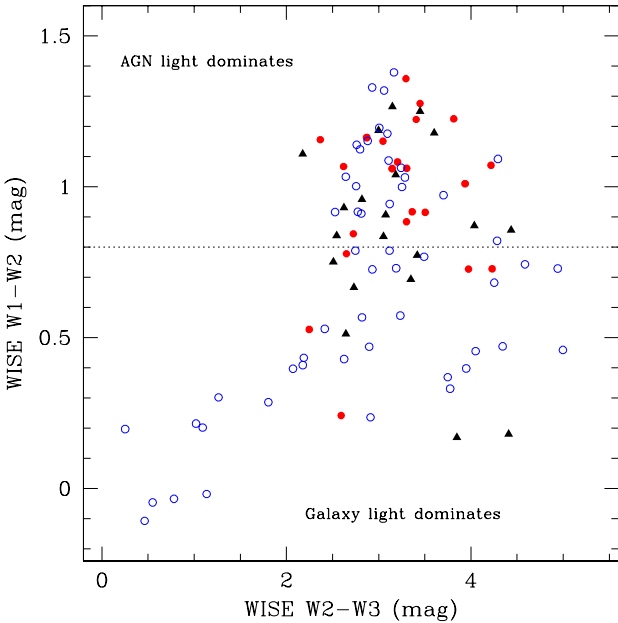


**Figure 4.** A WISE two-colour diagram similar to Figure 3, but now split into strongly-scintillating sources (red filled circles), moderately scintillating sources (black triangles), and sources showing weak or no scintillation (open blue circles).

**Table 6.** Overview of the WISE properties of sources in the main IPS-FIRST sample (Table 3).

IPS	n	Fraction w. WISE ID	Median W1 (mag)
All sources	88	91% (80/88)	15.81 $\pm 0.21$
Weak/no scint. (NSI < 0.4)	40	93% (37/40)	15.37 $\pm 0.35$
Moderate scint. ( $0.4 \leq \text{NSI} < 0.9$ )	18	83% (15/18)	15.94 $\pm 0.43$
Strong scint. (all w. NSI $\geq 0.9$ )	14	86% (12/14)	16.45 $\pm 0.27$

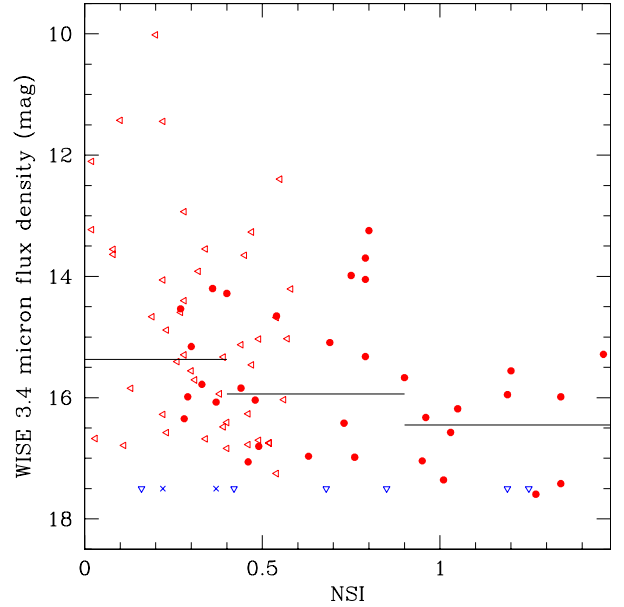


**Figure 5.** WISE W1 ( $3.4\mu\text{m}$ ) magnitude plotted against normalised scintillation index (NSI) for all objects in the main sample (Table 3). Red points show radio sources matched with a WISE counterpart - filled red points show objects with an IPS detection, while open triangles represent IPS non-detections with an upper limit in NSI. Blue points show sources not matched with WISE, for which we assume  $W1 < 17.5$  mag. Blue triangles show objects with IPS detections, and blue crosses objects with an upper limit in both W1 and NSI. The three horizontal black lines show the median W1 magnitudes for the three scintillation classes discussed in §2.3 of the text.

or (ii) the compact sub-sample could contain fewer QSOs (which are generally brighter in W1 than radio galaxies) than the extended sample. We consider this further in §3.2, where we discuss the relationship between W1 and redshift for the radio galaxy and QSO populations.

**Table 7.** Overview of the WISE properties of sources in the expanded compact sample (Table 4).

IPS	n	Fraction w. WISE ID	Median W1 (mag)
All sources (NSI $\geq 0.9$ )	65	91% (59/65)	16.33 $\pm 0.19$
Peaked-spectrum Callingham et al. (2017)	27	89% (24/27)	16.66 $\pm 0.34$
Compact steep spectrum ( $\alpha < -0.5$ )	33	91% (30/33)	16.38 $\pm 0.25$
Flat-spectrum ( $\alpha > -0.5$ )	5	100% (5/5)	15.86 $\pm 0.25$

### 3.1.3 The expanded compact source sample

Table 7 gives an overview of the WISE properties of the expanded compact sample from Table 4. The overall ID rate for these sources (91%) is similar to that for sources in the main IPS-FIRST sample (see Table 6).

Within the expanded compact sample, we can identify three sub-classes based on the low-frequency radio spectrum and 162-1400 MHz spectral index.

- **Compact steep-spectrum (CSS)** sources with power-law radio spectra and 162-1400 MHz spectral index  $\alpha < -0.5$ . 33 (51%) of the strongly-scintillating sources fall into this class

- **Peaked-spectrum sources:** 27 (42%) of the strongly-scintillating (NSI  $\geq 0.9$ ) sources in the expanded compact sample are peaked-spectrum objects identified by Callingham et al. (2017). As noted by Chhetri et al. (2018a), a surprisingly high fraction of all compact low-frequency sources have peaked radio spectra.

- **Compact flat-spectrum sources:** Only 7% of the strongly-scintillating sources have ‘flat’ radio spectra with 162-1400 MHz spectral index  $\alpha \geq -0.5$ . These flat-spectrum objects are a minority population and (as can be seen from Table 7) they are significantly brighter in W1 than the other compact sources. Three of the five objects in this class are known to be QSOs. The other two have no optical spectrum currently available.

Both the compact steep-spectrum and peaked-spectrum sub-samples contain many objects with faint W1 magnitudes. The median W1 magnitudes for both classes are similar - implying that we see a genuine distinction between a majority population of steep- and peaked-spectrum compact sources associated with (mainly) faint galaxies, and a smaller population of flat-spectrum sources associated mainly with radio-loud QSOs. Our current sample has only two strongly-scintillating sources with  $\alpha < -1$  (i.e. ‘ultra-steep spectrum’ sources as defined by Jarvis et al. (2001a)), but we note that only four of the seven compact steep-spectrum sources with  $\alpha < -0.9$  (57%) have a WISE ID, suggesting that many strongly-scintillating sources with very steep spectra may lie at high redshift. A larger sample is clearly needed to test this further. An investigation of the radio source counts for different sub-populations of strongly scintillating sources is

**Table 8.** Overview of the WISE properties of sources in the IPS-MRC-1 Jy sample (Table 5).

IPS	n	Fraction w. WISE ID	Median W1 mag
All sources	85	95% (81/85)	15.45 $\pm 0.25$
Weak/no scint. (NSI $< 0.4$ )	53	96% (51/53)	15.10 $\pm 0.34$
Moderate scint. ( $0.4 \leq \text{NSI} < 0.9$ )	18	94% (17/18)	15.68 $\pm 0.44$
Strong scint. (all w. NSI $\geq 0.9$ )	8	88% (7/8)	16.64 $\pm 0.81$
All QSOs (Kapahi et al. 1998b)	14	100% (14/14)	14.16 $\pm 0.43$
All galaxies (McCarthy et al. 1996)	71	88% (67/71)	15.56 $\pm 0.28$

presented in a companion paper by Chhetri et al. (2018b); Paper III in this series.

### 3.1.4 The IPS-MRC-1 Jy sample

Table 8 summarises the properties of the hosts of radio sources in the IPS-MRC-1Jy sample, 84% of which are classified as galaxies and 16% as radio-loud QSOs. It is notable that of the 14 QSOs in the sample, only one (MRC 0040-208 at  $z=0.655$ ) is a strongly scintillating source with NSI  $\geq 0.9$ .

The MRC-1Jy sample can be reliably divided into sub-samples of radio galaxies and QSOs, so we can now address the issue raised in §3.1.2 of whether the median W1 magnitude of strongly-scintillating sources is fainter because the objects are more distant, or because the samples contain a different mix of (fainter) galaxies and (brighter) QSOs. Table 9 lists the median W1 magnitude and 162-1400 MHz spectral index for the radio galaxies in the MRC sample, with QSOs excluded.

The  $\sim 1.5$  mag difference in median W1 magnitude between the hosts of weakly-scintillating and strongly-scintillating sources remains when QSOs are excluded from the calculation. From this, we conclude that the difference is not due to a different mix of (brighter) QSOs and (fainter) galaxies as suggested in §3.1.2. Instead, it must arise either because the strongly-scintillating sources are more distant or because their host galaxies are less luminous at mid-IR wavelengths. To resolve this, we now consider what is known about the redshift distribution of the IPS sources.

## 3.2 Estimated redshift distribution for the compact low-frequency sources

The K-z relation between the near-infrared K-band magnitude and redshift of powerful radio galaxies (e.g. Willott et al. 2003) is commonly used to estimate the redshift of radio galaxies if a spectroscopic redshift measurement is not available. For the large-area Chhetri et al. (2018a) IPS field, mid-infrared data from the WISE survey are significantly deeper than the available K-band data from the 2MASS

**Table 9.** Median W1 magnitude and 162-1400 MHz radio spectral index for galaxies in the IPS-MRC-1 Jy sample (with QSOs excluded).

IPS	n	Median	
		W1 mag	$\alpha$
Weak/no scint. (NSI < 0.4)	43	15.33 $\pm 0.41$	-0.78 $\pm 0.05$
Moderate scint. (0.4 $\leq$ NSI < 0.9)	15	15.79 $\pm 0.33$	-0.80 $\pm 0.05$
Strong scint. (all w. NSI $\geq$ 0.9)	7	16.92 $\pm 0.53$	-0.78 $\pm 0.13$

survey, so we investigated the use of the WISE W1 magnitude as an alternative redshift indicator. Like the  $2.2\mu\text{m}$  K-band, the  $3.4\mu\text{m}$  WISE W1 band mainly tracks the light of the stellar population in normal galaxies, so there is a reasonable justification for the use of the W1 magnitude as a photometric redshift estimator for radio galaxies in the same way that K-band (Willott et al. 2003) and  $r$ -band (Burgess & Hunstead 2006b) have previously been used.

The observed K–W1 colour of a galaxy will change significantly with redshift, due to differing  $k$ -corrections in the K and W1 bands (Jarrett et al. 2017), so making a direct conversion from the well-established K– $z$  relation to a new W1– $z$  relation is not straightforward. Instead, we chose to derive a simple empirical relation between W1 and redshift that we can use to estimate the likely redshift distribution of the strongly-scintillating radio sources in the Chhetri et al. (2018a) IPS field.

### 3.2.1 The W1– $z$ relation for radio galaxies

Figure 6 plots WISE W1 magnitude against spectroscopic redshift for objects in Tables 3, 4 and 5 that have a reliable redshift measurement in the literature. A limit of  $W1 > 17.5$  mag is assumed for the small number of sources with no catalogued W1 magnitude.

Strongly-scintillating sources with known redshifts are marked by open circles in Figure 6. The red points for galaxy hosts of strongly-scintillating sources follow the same W1– $z$  relation as the host galaxies of other sources in the field. From this, we conclude that the fainter W1 magnitudes found for strongly-scintillating sources in §3.1.4 (see Table 9) arise mainly because the strongly-scintillating sources are more distant, and not because their host galaxies are less luminous than those of other bright low-frequency radio sources.

The dashed line in Figure 6 shows the relation

$$W1 = 15.860 + 2.976 \log(z), \quad (1)$$

which represents a simple linear fit to the galaxy points in Figure 6. The results shown here imply that powerful radio galaxies with  $W1 > 16.8$  mag are likely to lie at redshift  $z > 2$ . This appears reasonably consistent with our expectations from the Willott et al. (2003) K– $z$  relation:

$$K = 17.37 + 4.53 \log(z) - 0.31 \log(z)^2, \quad (2)$$

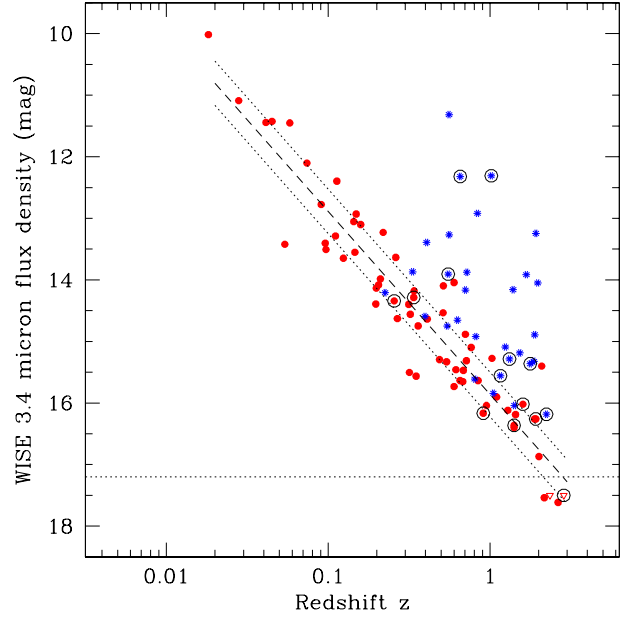


**Figure 6.** WISE W1 ( $3.4\mu\text{m}$ ) magnitude plotted against redshift for objects in Tables 3, 4 or 5 that have a reliable spectroscopic redshift available in the literature. Red points show galaxies, and blue points QSOs. The dotted horizontal line at  $W1 = 17.2$  mag shows the completeness limit of the WISE catalogue, and the two red triangles below this line are upper limits in W1 for objects not detected in WISE. Open black circles show compact sources with strong IPS ( $\text{NSI} \geq 0.9$ ). The dashed line is a simple linear fit to the data points for galaxies, as discussed in the text. Offsets of  $\pm 0.36$  mag from this line are also shown, and correspond to the median scatter of galaxies about the fitted line.

given the strong redshift dependence of the observed (K–W1) colour due to band-shifting effects (see Figure 8b of Jarrett et al. 2017).

### 3.2.2 Redshift estimates for the strongly-scintillating IPS sources

We now use the W1– $z$  relation from equation (1) to estimate the likely redshift distribution for the strongly-scintillating sources in the Chhetri et al. (2018a) IPS field. We caution that these redshift estimates are intended to be indicative only. In particular, the sources in the IPS sample are a mixture of galaxies and QSOs and so a W1– $z$  relation based on galaxy data only provides a lower limit to the redshift of an individual radio source of unknown type.

Table 10 summarizes the results. The estimated median redshift for all sources in the main IPS-FIRST sample is  $z \sim 1.0$ , roughly consistent with what is expected for sources in a survey of this depth at 162 MHz (e.g. Condon et al. 1998). 20% of these sources have a host galaxy with  $W1 > 16.8$  mag, and are expected to be high-redshift radio galaxies (HzRGs) at redshift  $z > 2$ . Sources that show weak or no scintillation have a significantly lower median redshift than the sample as a whole.

The strongly-scintillating sources in the expanded compact sample are significantly more distant than the overall low-frequency source population, with an estimated median



**Table 10.** Estimated median redshifts for different source classes. The final column lists the fraction of sources with  $W1 > 16.8$  mag, i.e. sources for which the estimated redshift is  $z > 2$ .

IPS	n	median W1 mag	median $z_{\text{est}}$	W1 > 16.8
<b>Main IPS-FIRST sample</b>				
All sources	88	15.81 $\pm 0.21$	0.96 $\pm 0.18$	20%
Weak/no scint. (NSI < 0.4)	40	15.37 $\pm 0.35$	0.68 $\pm 0.20$	8%
<b>Expanded compact sample</b>				
All with NSI $\geq 0.9$	65	16.33 $\pm 0.19$	1.44 $\pm 0.26$	37%
Peaked-spectrum	27	16.66 $\pm 0.34$	1.86 $\pm 0.53$	48%
Compact steep spectrum	33	16.38 $\pm 0.25$	1.50 $\pm 0.33$	33%
<b>IPS-MRC-1Jy sample</b>				
All galaxies	71	15.56 $\pm 0.28$	0.79 $\pm 0.18$	17%
Galaxies w. redshifts	41	15.28 $\pm 0.39$	0.64 $\pm 0.21$	12%
Galaxies w. redshifts	Median $z_{\text{spec}} = 0.60$			
Galaxies w. redshifts	Fraction with $z_{\text{spec}} > 2 = 15\%$			

redshift of  $z \sim 1.5$ . At least one-third of all these sources have hosts that are fainter than 16.8 mag in W1, and so are expected to lie at  $z > 2$ .

Finally, if we examine the subset of the IPS-MRC-1Jy sample for which reliable spectroscopic redshifts are available, we see a reassuring consistency between the W1-based estimates and spectroscopic measurements of both the median redshift and the fraction of sources likely to lie at  $z > 2$ . The former is probably to be expected, since MRC spectroscopic redshifts were used (along with other data) to derive the W1- $z$  relation presented in §3.2.1. However, the agreement between the estimated and actual fraction of MRC-1Jy galaxies at redshift  $z > 2$ , both of which represent the tail of a distribution, is encouraging and suggests that IPS might potentially be used as a new tool to identify high-redshift radio galaxies (HzRGs) in the distant Universe. We explore this idea further in the next section.

## 4 IPS AS A TOOL FOR SELECTING HIGH-REDSHIFT RADIO GALAXIES?

### 4.1 An IPS-based selection method for HzRGs

Current methods for identifying high-redshift radio galaxies (HzRGs) at  $z > 2$  generally involve the selection of sources with ultra-steep (USS) radio spectra (e.g. spectral index  $\alpha < -1.3$ ; Miley & De Breuck (2008)). Secondary criteria related to the angular size of the radio source and faintness of the host galaxy are also applied. Studies based on this technique (van Breugel et al. 1999; Jarvis et al. 2001b; De Breuck et al. 2002; Bryant et al. 2009; Saxena et al. 2018) have been effective in selecting distant objects, but do not necessarily give a complete and unbiased picture of the high-redshift radio-source population. For example, most of

the distant objects selected through the USS technique have radio emission extending over tens of kiloparsecs (Miley & De Breuck 2008), suggesting that this technique may bias against the selection of young, compact radio galaxies.

An IPS-based technique for selecting HzRG candidates could provide a useful alternative to traditional USS methods. In particular:

- Selecting strongly-scintillating sources dominated by a compact (sub-arcsec) radio component simplifies the process of identifying the host galaxy. For example, McCarthy et al. (1996) note that identification of the hosts of compact (angular size  $\leq 5$  arcsec) and unresolved radio sources in their MRC-1Jy sample was straightforward, whereas more extended sources sometimes had two or more plausible identifications for which follow-up spectra were needed.

- The IPS technique typically selects sources with angular size  $\leq 0.5$  arcsec, corresponding to linear scales smaller than 3–5 kpc at redshift  $z > 2$ . In other words, this technique should select objects with linear size similar to classical GPS and CSS radio galaxies (O’Dea 1998). While this is only a transient stage in the evolution of an individual radio galaxy, it is a stage that all powerful radio galaxies are expected to pass through – allowing us to connect objects in the same evolutionary phase at different redshifts. Since the USS technique often picks up more extended lobe-dominated radio galaxies, the USS and IPS techniques have the potential to be complementary in building up complete samples of high-redshift radio sources.

- The median estimated redshift of  $z \sim 1.5$  for the compact sources in Table 10 is not far below the median value of  $z \sim 1.9$  for the Jarvis et al. (2001a) 6C\* sample, which used USS spectral-index selection (with  $\alpha < -0.98$  at 151–4850 MHz). The IPS technique may therefore be able to reach a comparable redshift depth to previous USS searches, but without the need to impose any spectral-index selection.

An IPS-based technique for identifying HzRG candidates using data from a wide-field IPS survey with the MWA would be a fairly straightforward process:

- Select strongly-scintillating radio sources using an appropriate cutoff in the normalised scintillation index.
- Cross-match the NVSS or SUMSS radio positions of these sources with the allWISE mid-IR survey catalogue, and select objects fainter than some appropriate limit in W1 magnitude.

In the next section, we use the IPS-MRC-1Jy sample to make some first tests of the effectiveness and completeness of this IPS-based HzRG search technique.

### 4.2 Tests on the MRC-1Jy sample

For a HzRG search technique to be effective, it should ideally perform well against two measures:

- Efficiency:** What fraction of the selected candidates are in the desired redshift range (e.g. what fraction are at  $z > 2$ )?
- Completeness:** What fraction of all sources in the target redshift range are selected by the technique?

The IPS-MRC-1Jy sample contains six  $z > 2$  radio AGN that were selected from a flux-limited survey without any

spectral-index preselection, so we can use this sample to test the efficiency and completeness of the proposed IPS technique. Since this  $z > 2$  sample is very small, the results are only indicative at this stage. With IPS observations of the full MRC-1Jy survey area, more detailed tests would be possible.

As a starting point, we assume the two selection criteria to be  $\text{NSI} > 0.8$ , and  $W1 > 17.2$  mag. We chose this slightly lower cutoff in NSI partly based on the distribution of points in Figure 5, but also to avoid reducing the size of our small test sample even further. The results were as follows:

(i) IPS Efficiency: Of the 55 sources in Table 5 with reliable redshift data, only two (MRC 0030-219 and MRC 0052-241) satisfy both selection criteria. These two objects both lie at  $z > 2$  ( $z = 2.168$  and  $2.86$  respectively). Thus the IPS technique appears to be very efficient based on this small sample.

(ii) IPS Completeness: Of the six  $z > 2$  radio galaxies in the IPS-MRC-1Jy sample, two were identified by the IPS-based selection criteria, giving a completeness of  $\sim 30\%$ .

We can make similar tests for the USS-based selection techniques used by Jarvis et al. (2001b) and Saxena et al. (2018).

(i) USS Efficiency: Three of the 55 sources with redshifts in Table 5 (MRC 0015-229, MRC 0052-241 and MRC 0140-257) satisfied the Jarvis et al. (2001b) selection criterion of  $\alpha < -0.98$ . All three objects lie at  $z > 2$  ( $z = 2.01$ ,  $2.86$  and  $2.64$  respectively). Thus the Jarvis et al. (2001b) USS technique also appears to be very efficient. No source in Table 5 has a steep enough radio spectrum to satisfy the Saxena et al. (2018) cutoff of  $\alpha < -1.3$ .

(ii) USS Completeness: Of the six  $z > 2$  radio galaxies in the IPS-MRC-1Jy sample, three satisfied the Jarvis et al. (2001b) selection criterion of  $\alpha < -0.98$  giving a completeness of  $\sim 50\%$ . None of the six  $z > 2$  sources satisfied the Saxena et al. (2018) selection criteria (which were designed for use with much deeper radio surveys), so the completeness for this more stringent USS cutoff of  $\alpha < -1.3$  is  $< 17\%$ .

Our conclusion from these tests (on an admittedly small sample) is that the IPS selection technique appears competitive with existing USS techniques in terms of efficiency and completeness. The IPS technique also has the advantage of being able to select high-redshift radio AGN candidates without any need for spectral-index preselection. Extending the work presented here to a larger IPS sample with additional redshift data would allow the performance of this technique to be tested in more detail.

## 5 CONCLUSIONS AND FUTURE WORK

In this paper, we have identified the hosts of a representative sample of radio sources for which Interplanetary Scintillation (IPS) measurements have been made by Chhetri et al. (2018a). We have also shown that WISE mid-IR magnitudes can provide a useful redshift estimator for these powerful radio galaxies, using only a simple linear relation between  $W1$  and  $\log(z)$  (see Figure 6).

The hosts of sub-arcsecond compact sources identified through their strong scintillation in MWA IPS observations

are typically distant radio galaxies (median redshift  $z \sim 1.5$ ), and we estimate that over 30% of them lie at redshift  $z > 2$ . More follow-up optical/IR data, and a larger-area IPS survey are needed to take this work further, but the results to date look very encouraging.

In the near future, the upgraded capabilities of the MWA should allow wide-field IPS studies to probe significantly deeper in flux density - reaching a typical detection limit of 0.4 Jy at 162 MHz, and detecting sources as weak as 0.1 Jy under ideal conditions (Morgan et al. (2018a); Paper V in this series). This should allow us to probe to even higher redshift, and potentially detect powerful compact radio galaxies and radio-loud QSOs out to redshift 5-6.

## ACKNOWLEDGEMENTS

This scientific work makes use of the Murchison Radio-astronomy Observatory, operated by CSIRO. We acknowledge the Wajarri Yamatji people as the traditional owners of the Observatory site. Support for the operation of the MWA is provided by the Australian Government (NCRIS), under a contract to Curtin University administered by Astronomy Australia Limited. We acknowledge the Pawsey Supercomputing Centre which is supported by the Western Australian and Australian Governments.

Parts of this research were conducted by the Australian Research Council Centre of Excellence for All-sky Astrophysics (CAASTRO), through project number CE110001020.

This publication makes use of data products from the Wide-field Infrared Survey Explorer, which is a joint project of the University of California, Los Angeles, and the Jet Propulsion Laboratory/California Institute of Technology, funded by the National Aeronautics and Space Administration.

Funding for the Sloan Digital Sky Survey IV has been provided by the Alfred P. Sloan Foundation, the U.S. Department of Energy Office of Science, and the Participating Institutions. SDSS-IV acknowledges support and resources from the Center for High-Performance Computing at the University of Utah. The SDSS web site is [www.sdss.org](http://www.sdss.org).

SDSS-IV is managed by the Astrophysical Research Consortium for the Participating Institutions of the SDSS Collaboration including the Brazilian Participation Group, the Carnegie Institution for Science, Carnegie Mellon University, the Chilean Participation Group, the French Participation Group, Harvard-Smithsonian Center for Astrophysics, Instituto de Astrofísica de Canarias, The Johns Hopkins University, Kavli Institute for the Physics and Mathematics of the Universe (IPMU) / University of Tokyo, Lawrence Berkeley National Laboratory, Leibniz Institut für Astrophysik Potsdam (AIP), Max-Planck-Institut für Astronomie (MPIA Heidelberg), Max-Planck-Institut für Astrophysik (MPA Garching), Max-Planck-Institut für Extraterrestrische Physik (MPE), National Astronomical Observatories of China, New Mexico State University, New York University, University of Notre Dame, Observatório Nacional / MCTI, The Ohio State University, Pennsylvania State University, Shanghai Astronomical Observatory, United Kingdom Participation Group, Universidad Nacional Autónoma de México, University of Arizona, University

of Colorado Boulder, University of Oxford, University of Portsmouth, University of Utah, University of Virginia, University of Washington, University of Wisconsin, Vanderbilt University, and Yale University.

## REFERENCES

- Abolfathi B., et al., 2018, *ApJS*, **235**, 42
- Acerro F., et al., 2015, *ApJS*, **218**, 23
- Baker J. C., Hunstead R. W., Kapahi V. K., Subrahmanya C. R., 1999, *ApJS*, **122**, 29
- Becker R. H., White R. L., Helfand D. J., 1995, *ApJ*, **450**, 559
- Best P. N., Röttgering H. J. A., Lehnert M. D., 1999, *MNRAS*, **310**, 223
- Best P. N., Kauffmann G., Heckman T. M., Ivezić Ž., 2005, *MNRAS*, **362**, 9
- Bolton J. G., Wall J., Shimmings A. J., 1971, *Australian Journal of Physics*, **24**, 889
- Bryant J. J., Johnston H. M., Broderick J. W., Hunstead R. W., De Breuck C., Gaensler B. M., 2009, *MNRAS*, **395**, 1099
- Burgess A. M., Hunstead R. W., 2006a, *AJ*, **131**, 100
- Burgess A. M., Hunstead R. W., 2006b, *AJ*, **131**, 114
- Callingham J. R., et al., 2017, *ApJ*, **836**, 174
- Chhetri R., Morgan J., Ekers R. D., Macquart J.-P., Sadler E. M., Giroletti M., Callingham J. R., Tingay S. J., 2018a, *MNRAS*, **474**, 4937
- Chhetri R., Ekers R. D., Morgan J., Macquart J.-P., Franzen T. M. O., 2018b, *MNRAS*, **479**, 2318
- Ching J. H. Y., et al., 2017, *MNRAS*, **464**, 1306
- Condon J. J., Cotton W. D., Greisen E. W., Yin Q. F., Perley R. A., Taylor G. B., Broderick J. J., 1998, *AJ*, **115**, 1693
- Coppejans R., Cseh D., Williams W. L., van Velzen S., Falcke H., 2015, *MNRAS*, **450**, 1477
- Cutri R. M., et al., 2013, Explanatory Supplement to the All-WISE Data Release Products. <http://wise2.ipac.caltech.edu/docs/release/allwise/expsup/index.html>
- De Breuck C., van Breugel W., Stanford S. A., Röttgering H., Miley G., Stern D., 2002, *AJ*, **123**, 637
- Drake C. L., McGregor P. J., Dopita M. A., van Breugel W. J. M., 2003, *AJ*, **126**, 2237
- Dunlop J. S., Peacock J. A., Savage A., Lilly S. J., Heasley J. N., Simon A. J. B., 1989, *MNRAS*, **238**, 1171
- Emonts B. H. C., et al., 2015, *MNRAS*, **451**, 1025
- Emonts B. H. C., et al., 2016, *Science*, **354**, 1128
- Glowacki M., Allison J. R., Sadler E. M., Moss V. A., Jarrett T. H., 2017, preprint, ([arXiv:1709.08634](https://arxiv.org/abs/1709.08634))
- Gürkan G., Hardcastle M. J., Jarvis M. J., 2014, *MNRAS*, **438**, 1149
- Heckman T. M., Best P. N., 2014, *ARA&A*, **52**, 589
- Hook I. M., Shaver P. A., Jackson C. A., Wall J. V., Kellermann K. I., 2003, *A&A*, **399**, 469
- Hurley-Walker N., et al., 2017, *MNRAS*, **464**, 1146
- Jarrett T. H., et al., 2017, *ApJ*, **836**, 182
- Jarvis M. J., et al., 2001a, *MNRAS*, **326**, 1563
- Jarvis M. J., Rawlings S., Eales S., Blundell K. M., Bunker A. J., Croft S., McLure R. J., Willott C. J., 2001b, *MNRAS*, **326**, 1585
- Jones D. H., et al., 2009, *MNRAS*, **399**, 683
- Kapahi V. K., Athreya R. M., van Breugel W., McCarthy P. J., Subrahmanya C. R., 1998a, *ApJS*, **118**, 275
- Kapahi V. K., Athreya R. M., Subrahmanya C. R., Baker J. C., Hunstead R. W., McCarthy P. J., van Breugel W., 1998b, *ApJS*, **118**, 327
- Laing R. A., Riley J. M., Longair M. S., 1983, *MNRAS*, **204**, 151
- Massaro F., D’Abrusco R., Tosti G., Ajello M., Gasparri D., Grindlay J. E., Smith H. A., 2012, *ApJ*, **750**, 138
- McCarthy P. J., van Breughel W., Kapahi V. K., Subrahmanya C. R., 1991, *AJ*, **102**, 522
- McCarthy P. J., Kapahi V. K., van Breugel W., Persson S. E., Athreya R., Subrahmanya C. R., 1996, *ApJS*, **107**, 19
- Miley G., De Breuck C., 2008, *A&ARv*, **15**, 67
- Morgan J. S., Macquart J., Chhetri R., Ekers R. D., Tingay S. J., Sadler E. M., 2018a, preprint, ([arXiv:1809.09388](https://arxiv.org/abs/1809.09388))
- Morgan J. S., et al., 2018b, *MNRAS*, **473**, 2965
- Murphy T., et al., 2010, *MNRAS*, **402**, 2403
- O’Dea C. P., 1998, *PASP*, **110**, 493
- O’Dea C. P., Owen F. N., 1985, *AJ*, **90**, 927
- Osmer P. S., Porter A. C., Green R. F., 1994, *ApJ*, **436**, 678
- Saxena A., et al., 2018, *MNRAS*, **475**, 5041
- Schmidt M., 1965, *ApJ*, **141**, 1
- Tingay S. J., et al., 2013, *Publ. Astron. Soc. Australia*, **30**, e007
- Titov O., Jauncey D. L., Johnston H. M., Hunstead R. W., Christensen L., 2011, *AJ*, **142**, 165
- Wayth R. B., et al., 2015, *Publ. Astron. Soc. Australia*, **32**, e025
- Wegner G., Colless M., Saglia R. P., McMahan R. K., Davies R. L., Burstein D., Baggley G., 1999, *MNRAS*, **305**, 259
- Willott C. J., Rawlings S., Jarvis M. J., Blundell K. M., 2003, *MNRAS*, **339**, 173
- Wills D., Wills B. J., 1976, *ApJS*, **31**, 143
- Wold M., Lacy M., Lilje P. B., Serjeant S., 2000, *MNRAS*, **316**, 267
- Wright A. E., Ables J. G., Allen D. A., 1983, *MNRAS*, **205**, 793
- Wright E. L., et al., 2010, *AJ*, **140**, 1868
- de Vaucouleurs G., de Vaucouleurs A., Corwin Jr. H. G., Buta R. J., Paturel G., Fouqué P., 1991, Third Reference Catalogue of Bright Galaxies. Volume I: Explanations and references. Volume II: Data for galaxies between  $0^h$  and  $12^h$ . Volume III: Data for galaxies between  $12^h$  and  $24^h$ . Publ: Springer, New York, NY (USA).
- van Breugel W., De Breuck C., Stanford S. A., Stern D., Röttgering H., Miley G., 1999, *ApJ*, **518**, L61
- van Velzen S., Falcke H., Körding E., 2015, *MNRAS*, **446**, 2985

**Table 3.** The main IPS-FIRST sample of high S/N sources from the Chhetri et al. (2018a) IPS sample that lie within the FIRST overlap area.

GLEAM name	Alt name	$S_{162}$ Jy	$\pm$ Jy	Norm SNR	NSI	FIRST comp	Radio class	Radio position (J2000)		WISE match	W1 mag	$\pm$	z	$z_{\text{red}}$	Notes
(1)	(2)	(3)	(4)	(5)	(6)	(7)	(8)	RA	Dec	(11)	(12)	(13)	(14)	(15)	(16)
<b>(a) All high S/N sources in the FIRST survey area (NormSNR <math>\geq 12.5</math>)</b>															
J000057-105435	PKS 2358-111	4.775	0.023	23.1	0.63	1	Single	00 00 57.662	-10 54 32.16	J000057.57-105432.1	16.966	0.134	..	..	
J000829-055839	3C 003	7.643	0.018	27.6	0.79	1	Single	00 08 29.354	-05 58 45.91	J000829.30-055845.2	13.698	0.026	..	..	
J001356-091952	PKS 0011-096	4.131	0.020	25.9	< 0.28	4	Double	00 13 56.86	-09 19 52.59	J001357.24-091949.5	15.295	0.041	0.4878	SDSS	★ A
J001454-095911	PKS 0012-102	2.136	0.020	16.0	< 0.31	2	Double	00 14 54.91	-09 59 12.8	J001454.97-095912.2	15.708	0.048	..	..	
J001821-111139	MRC 0015-114	1.932	0.020	16.2	0.95	1	Single	00 18 22.052	-11 11 38.87	J001821.92-111139.1	17.042	0.128	..	..	
J001859-102248	PKS 0016-10	7.648	0.020	57.8	0.44	2	Double	00 18 59.48	-10 22 49.2	J001859.52-102245.6	15.843	0.053	..	..	
J001931-043543	3C 007	4.523	0.018	16.4	1.03	1	Single	00 19 31.513	-04 35 47.07	J001931.48-043548.1	16.573	0.087	..	..	
J002050-085731	PKS 0018-09	6.327	0.019	42.3	0.29	2	Double	00 20 50.33	-08 57 34.9	J002050.13-085733.5	15.986	0.062	..	..	
J002208-104133	PKS 0019-109	1.774	0.019	14.3	1.34	1	Single	00 22 09.010	-10 41 33.29	J002209.00-104132.1	17.419	0.175	..	..	P
J002223-070230	PKS 0019-073	3.821	0.016	23.1	1.25	1	Single	00 22 23.050	-07 02 35.23	..	..	..	..	★ P	
J002319-074445	PKS 0020-08	5.470	0.017	32.9	0.27	1	Single (ext)	00 23 19.031	-07 44 49.69	J002319.02-074449.3	14.534	0.031	0.514	SDSS	A
J002533-064253	MRC 0023-069	2.226	0.015	15.1	< 0.03	3	Triple	00 25 33.751	-06 43 02.19	J002533.77-064301.0	16.673	0.095	..	..	
J002631-084234	PKS 0024-089	2.253	0.019	16.4	< 0.22	2	Double	00 26 31.60	-08 42 37.0	J002631.46-084235.5	14.058	0.029	..	..	A
J002922-111151	PKS 0026-114	3.822	0.018	38.8	0.73	1	Single	00 29 22.615	-11 11 51.28	J002922.68-111150.9	16.420	0.075	..	..	
J003102-091157	PKS 0028-094	1.963	0.020	15.7	< 0.40	2	Double	00 31 03.00	-09 12 04.2	J003102.89-091202.4	16.408	0.075	..	..	
J003201-085133	PKS 0029-091	2.125	0.020	16.6	1.27	1	Single	00 32 00.977	-08 51 37.48	J003200.97-085139.1	17.593	0.212	..	..	P
J003217-034903	PKS 0029-040	3.779	0.017	15.2	< 0.34	2	Double	00 32 17.32	-03 49 08.4	J003217.22-034909.1	13.548	0.030	..	..	
J003251-101801	MRC 0030-105	1.659	0.019	14.5	< 0.37	2	Double	00 32 51.91	-10 18 05.0	..	..	..	..	★	
J003354-073019	PKS 0031-07	6.134	0.017	47.8	0.33	2	Double	00 33 54.66	-07 30 28.6	J003354.74-073029.7	15.781	0.051	..	..	
J003502-083437	MRC 0032-088	2.360	0.019	21.2	0.36	3	Triple	00 35 02.72	-08 34 37.38	J003503.45-083440.1	14.200	0.029	..	..	
J003616-111650	PKS 0033-115	1.837	0.019	21.0	0.30	4	Double	00 36 16.81	-11 16 50.58	J003615.94-111657.8	15.157	0.041	..	..	
J003704-010910	3C 015	19.710	0.024	35.8	< 0.02	3	Triple	00 37 03.959	-01 09 04.45	J003704.10-010908.2	12.103	0.024	0.0737	SDSS	A
J003820-020737	3C 017	28.389	0.026	60.7	< 0.02	3	Triple	00 38 20.30	-02 07 37.5	J003820.53-020740.5	13.228	0.024	0.2204	SDSS	A
J003822-111244	PMN J0038-1112	1.347	0.018	15.4	< 0.39	1	Single (ext)	00 38 22.781	-11 12 48.27	J003822.80-111250.2	15.331	0.041	..	..	
J003924-080223	MRC 0036-083	1.520	0.016	13.4	< 0.47	1	Single (ext)	00 39 25.019	-08 02 25.59	J003924.98-080227.0	15.459	0.043	0.6165	SDSS	
J003938-074610	MRC 0037-080	2.493	0.017	23.1	< 0.39	1	Single (ext)	00 39 38.245	-07 46 10.74	J003938.31-074610.9	16.480	0.080	..	..	
J004049-094832	MRC 0038-100	2.173	0.022	19.6	0.42	2	Double	00 40 48.56	-09 48 30.9	..	..	..	..	★	
J004125-014314	PKS 0038-019	7.811	0.021	17.5	< 0.32	2	Double	00 41 26.02	-01 43 16.0	J004126.00-014315.7	13.915	0.027	1.679	Du89	A
J004232-081543	MRC 0040-085	2.296	0.018	21.3	< 0.34	2	Double	00 42 32.26	-08 15 48.1	J004232.23-081548.8	16.680	0.090	..	..	
J004246-061325	PKS 0040-06	2.237	0.016	15.6	< 0.45	2	Double	00 42 46.84	-06 13 53.0	J004246.84-061353.0	13.649	0.025	0.1243	SDSS	★

GLEAM name	Alt name	$S_{162}$ Jy	$\pm$ Jy	Norm SNR	NSI	FIRST comp	Radio class	Radio position (J2000)		WISE match	W1 mag	$\pm$	$z$	$z_{\text{ref}}$	Notes
(1)	(2)	(3)	(4)	(5)	(6)	(7)	(8)	RA (9)	Dec (10)	(11)	(12)	(13)	(14)	(15)	(16)
J004409-050659	PKS 0041-053	2.652	0.016	17.2	< 0.52	1	Single (ext)	00 44 09.735	-05 07 03.02	J004409.82-050702.5	16.744	0.104	..	..	
J004644-052157	PKS 0044-05	2.933	0.016	21.2	0.79	1	Single	00 46 44.519	-05 22 00.29	J004644.54-052200.0	15.323	0.041	1.869	Wi76	
J004707-070451	PKS 0044-073	2.435	0.016	19.4	< 0.28	4	Double	00 47 07.86	-07 04 51.4	J004708.26-070445.4	14.400	0.029	..	..	
J004820-092212	MRC 0045-096	2.064	0.019	24.4	0.37	2	Double	00 48 20.65	-09 22 14.8	J004820.59-092215.4	16.074	0.063	..	..	
J004858-062832	PKS 0046-06	3.059	0.015	25.8	0.40	2	Double	00 48 58.40	-06 28 31.0	J004858.02-062831.0	14.282	0.028	..	..	
J004900-054358	MRC 0046-060	1.519	0.015	14.3	< 0.52	1	Single (ext)	00 49 00.852	-05 44 00.89	J004900.83-054400.5	16.752	0.097	..	..	
J004945-024257	PKS 0047-02	7.862	0.02	28.7	< 0.11	3	Triple	00 49 45.824	-02 42 59.99	J004945.33-024258.8	16.788	0.107	..	..	
J004954-100613	PKS 0047-10	2.257	0.018	27.3	1.05	1	Single	00 49 54.107	-10 06 14.95	J004954.03-100614.5	16.183	0.061	2.236	SDSS	A
J005039-102734	MRC 0048-107	2.138	0.018	26.8	0.90	1	Single	00 50 39.004	-10 27 35.77	..	15.67	0.05	..	..	★
J005049-032219	MRC 0048-036	3.230	0.020	17.0	< 0.54	2	Double	00 50 49.87	-03 22 21.5	J005049.96-032222.2	17.251	0.163	..	..	
J005108-065001	PKS 0048-071	1.773	0.016	16.9	0.79	1	Single	00 51 08.208	-06 50 02.25	J005108.20-065002.1	14.050	0.028	1.975	Wr83	AF
J005234-093819	MRC 0050-099	1.472	0.018	17.2	1.19	1	Single	00 52 34.551	-09 38 18.78	..	..	..	..	..	
J005354-092824	MRC 0051-097	1.634	0.019	18.9	< 0.08	4	Double	00 53 54.14	-09 28 24.1	J005354.20-092822.4	13.635	0.026	0.262	SDSS	
J005408-033354	3C 026	11.017	0.021	55.7	0.75	1	Single	00 54 08.433	-03 33 55.31	J005408.43-033355.2	13.984	0.028	0.2104	Sc65	A
J005447-091847	PKS 0052-096	1.890	0.019	22.7	< 0.26	1	Single (ext)	00 54 47.525	-09 18 48.04	J005447.42-091845.0	15.405	0.042	..	..	
J005447-095257	PMN J0054-0952	1.432	0.019	17.3	< 0.22	2	Double	00 54 47.81	-09 52 54.6	J005447.87-095254.6	16.276	0.068	..	..	
J005536-095216	MRC 0053-101	2.140	0.020	25.3	< 0.22	2	Double	00 55 36.69	-09 52 13.9	..	..	..	..	..	★
J005551-082956	MRC 0053-087	1.534	0.017	16.4	< 0.23	2	Double	00 55 51.66	-08 29 51.6	J005551.49-082953.8	14.885	0.033	0.7049	SDSS	
J005734-012329	3C 029	16.168	0.03	41.5	< 0.10	4	Wide double	00 57 34.92	-01 23 27.5	J005734.90-012327.5	11.425	0.022	0.0450	We99	★ A
J005805-053952	PKS 0055-059	1.994	0.016	14.8	0.69	1	Single	00 58 05.070	-05 39 52.45	J005805.08-053952.3	15.091	0.036	1.2456	Ti11	AF
J005903-075959	MRC 0056-082	1.355	0.016	16.9	< 0.46	2	Double	00 59 03.09	-07 59 59.2	J005903.11-080001.0	16.267	0.068	..	..	
J005928-101733	PMN J0059-1017	1.219	0.018	16.8	0.48	2	Double	00 59 29.10	-10 17 34.5	J005929.11-101734.8	16.04	0.056	1.419	SDSS	
J010042-050237	MRC 0058-053	1.91	0.016	13.2	1.34	1	Single	01 00 42.675	-05 02 36.84	J010042.64-050236.5	15.987	0.052	..	..	P
J010159-105555	TN J0102-1055	1.774	0.019	23.3	0.85	1	Single	01 02 00.001	-10 55 56.36	..	..	..	..	..	★
J010509-065250	PKS 0102-07	3.217	0.016	33.3	< 0.23	2	Wide double	01 05 09.44	-06 52 56.8	J010509.55-065257.1	16.577	0.072	..	..	
J010834-103346	PKS 0106-108	4.38	0.019	56.1	< 0.13	2	Wide double	01 08 34.62	-10 33 45.1	J010834.61-103345.7	15.844	0.048	..	..	
J010930-085303	PKS 0106-091	2.048	0.018	26.7	0.46	2	Double	01 09 30.32	-08 53 07.3	J010930.32-085304.9	17.060	0.114	..	..	
J011212-045504	MRC 0109-051	2.531	0.016	16.4	< 0.57	3	Triple	01 12 13.495	-04 55 10.76	J011213.45-045509.7	15.029	0.035	..	..	
J011242-080404	MRC 0110-083	1.987	0.017	23.0	< 0.19	2	Double	01 12 42.50	-08 04 02.3	J011242.72-080402.3	14.664	0.03	..	..	
J011312-101419	PKS 0110-105	1.565	0.019	20.2	1.46	1	Single	01 13 12.101	-10 14 21.57	J011312.09-101421.2	15.285	0.037	1.3210	SDSS	A
J011406-100800	PMN J0114-1007	1.135	0.020	15.4	0.49	1	Single (ext)	01 14 06.559	-10 08 01.00	J011406.33-100802.6	16.802	0.089	..	..	★
J011547-085756	PMN J0115-0857	1.076	0.019	13.3	< 0.46	3	Triple	01 15 47.404	-08 57 56.46	J011547.46-085756.8	16.772	0.098	..	..	A
J011645-041849	MRC 0114-045	2.007	0.017	12.6	< 0.27	1	Single (ext)	01 16 45.265	-04 18 54.84	J011645.21-041855.8	14.593	0.032	0.3965	SDSS	★
J011751-100557	PMN J0117-1006	1.125	0.020	13.2	< 0.40	2	Double	01 17 51.40	-10 05 53.0	J011751.35-100555.6	16.836	0.105	..	..	
J011815-012037	PKS 0115-01	5.357	0.020	16.4	1.20	1	Single	01 18 15.424	-01 20 30.12	J011815.39-012030.2	15.557	0.047	1.162	He 3	AP

Hosts of MWAG compact sources

GLEAM name	Alt name	S <sub>162</sub> Jy	± Jy	Norm SNR	NSI	FIRST comp	Radio class	Radio position (J2000)		WISE match	W1 mag	±	z	z <sub>ref</sub>	Notes
(1)	(2)	(3)	(4)	(5)	(6)	(7)	(8)	RA	Dec	(11)	(12)	(13)	(14)	(15)	(16)
J011931-102506	TXS 0117-106	1.194	0.020	15.9	< 0.49	1	Single	01 19 31.320	-10 25 08.72	J011931.25-102508.7	16.701	0.087	..	..	
J012227-042123	PKS 0119-04	4.770	0.018	29.6	0.80	1	Single	01 22 27.921	-04 21 27.19	J012227.88-042127.1	13.245	0.025	1.925	Os94	★ AP
J012231-061953	MRC 0120-065	1.573	0.017	14.1	< 0.49	4	Triple	01 22 32.00	-06 19 57.7	J012232.66-061958.5	15.034	0.034	..	..	★
J012434-040101	PKS 0122-042	3.128	0.018	17.9	< 0.47	3	Triple	01 24 34.794	-04 01 02.28	J012434.81-040102.7	13.267	0.024	0.5600	SDSS	A
J012603-012356	NGC 547	6.089	0.029	16.4	< 0.20	2	Complex	01 26 00.32	-01 20 42.6	J012600.61-012042.4	10.016	0.022	0.0182	RC3	★
J013029-083321	PKS 0127-08	1.786	0.02	15.8	< 0.44	2	Double	01 30 29.87	-08 33 19.9	J013029.94-083319.7	15.128	0.037	..	..	
J013136-070354	PKS 0129-073	8.868	0.021	62.6	0.16	2	Double	01 31 36.45	-07 03 57.3	..	..	..	..	..	★
J013157-081949	PKS 0129-085	2.183	0.02	17.8	< 0.28	3	Triple	01 31 57.572	-08 19 58.96	J013157.78-081954.9	12.931	0.023	0.1491	6dFGS	
J013212-065232	PKS 0129-07	5.309	0.02	36.7	1.19	1	Single	01 32 12.181	-06 52 35.92	J013212.24-065236.0	15.951	0.051	..	..	AP
J013325-102616	PKS 0130-106	1.168	0.02	12.9	< 0.55	2	Double	01 33 25.92	-10 26 17.3	J013325.87-102618.6	12.396	0.024	0.1132	SDSS	
J013524-051630	PKS 0132-055	2.048	0.017	14.0	< 0.58	7	Wide triple	01 35 23.741	-05 16 29.81	J013523.71-051629.8	14.208	0.027	0.225	SDSS	
J013635-080604	MRC 0134-083	2.644	0.021	18.4	< 0.08	2	Double	01 36 35.65	-08 06 04.2	J013635.64-080608.6	13.551	0.053	0.1464	6dFGS	
J013715-091141	MRC 0134-094	2.618	0.021	25.2	< 0.22	4	Complex	01 37 15.81	-09 11 41.8	J013715.38-091151.2	11.443	0.022	0.0413	We99	
J013716-093105	MRC 0134-097	1.503	0.022	13.0	< 0.56	2	Double	01 37 16.63	-09 31 12.0	J013716.67-093111.0	16.033	0.051	..	..	
J013800-053330	MRC 0135-058	2.313	0.018	15.2	< 0.54	3	Triple	01 38 00.80	-05 33 35.7	J013800.70-053335.5	14.677	0.029	..	..	
J013933-085023	MRC 0137-090	2.664	0.022	19.3	< 0.38	4	Double	01 39 33.22	-08 50 23.2	J013933.12-085027.0	15.937	0.052	..	..	
J014013-095654	PKS 0137-10	4.351	0.021	33.5	0.96	1	Single	01 40 12.840	-09 56 57.39	J014012.84-095657.7	16.327	0.066	..	..	AP
J014144-074607	MRC 0139-080	1.649	0.018	12.9	1.01	1	Single	01 41 43.986	-07 46 11.14	J014143.95-074611.4	17.357	0.133	..	..	
J014237-074232	PKS 0140-07	2.426	0.018	17.2	0.68	1	Single	01 42 36.440	-07 43 03.29	..	..	..	..	★	
J014645-053758	PKS 0144-05	4.351	0.02	17.5	0.54	1	single	01 46 45.124	-05 37 58.11	J014645.09-053759.2	14.654	0.03	0.63	Wo00	A
J015050-090126	PKS 0148-092	8.408	0.023	42.1	0.28	1	Single (ext)	01 50 50.384	-09 01 29.00	J015050.35-090126.9	16.348	0.06	..	..	A
J015142-103019	PKS 0149-107	5.21	0.02	29.7	< 0.30	2	Double	01 51 42.37	-10 30 20.5	J015142.29-103019.8	15.556	0.046	..	..	
J015323-033359	PKS 0150-03	8.399	0.021	20.0	0.76	1	Single	01 53 23.896	-03 33 59.31	J015323.84-033359.7	16.983	0.099	..	..	
<b>(b) Strongly-scintillating sources with intermediate S/N in the FIRST overlap area (NSI &gt; 0.90, 8.0 ≤ NormSNR &lt; 12.5)</b>															
J003931-111057	PMN J0039-1111	1.006	0.019	11.0	1.10	1	Single	00 39 31.591	-11 11 02.92	J003931.58-111102.6	13.907	0.027	0.5526	SDSS	A
J005315-070232	PMN J0053-0702	1.036	0.016	9.2	0.94	1	Single	00 53 15.689	-07 02 32.67	J005315.67-070232.5	16.313	0.069	..	..	
J010021-074718	MRC 0057-080	0.942	0.015	9.9	0.90	1	Single	01 00 21.063	-07 47 18.23	J010021.14-074718.4	16.771	0.099	..	..	
J011049-074142	PKS 0108-079	0.723	0.015	9.0	0.94	1	Single	01 10 50.018	-07 41 41.07	J011050.00-074141.1	15.362	0.039	1.776	Wr83	A
J011857-071855	MRC 0116-075	1.109	0.017	10.0	1.61	1	Single	01 18 57.486	-07 18 55.93	J011857.53-071855.6	16.656	0.087	..	..	P
J012102-094426	PMN J0121-0944	0.783	0.02	8.9	1.25	1	Single	01 21 02.078	-09 44 28.40	J012102.07-094428.6	16.144	0.063	..	..	

**Table columns:** (1) GLEAM name for the source; (2) Alternative name; (3) 162 MHz flux density in Jy, from [Chhetri et al. \(2018a\)](#); (4) Uncertainty in 162 MHz flux density; (5) Normalised S/N ratio from [Chhetri et al. \(2018a\)](#); (6) Normalised scintillation index, or an upper limit for sources where IPS was not detected; (7) Number of separate FIRST components associated with the GLEAM source; (8) Radio source classification; (9) Right Ascension used for WISE cross-matching (see text for details); (10) Declination used for WISE cross-matching; (11) Name of matched WISE source (if any); (12) WISE W1 magnitude; (13) Uncertainty in W1; (14) Optical spectroscopic redshift (if available); (15) Reference for optical redshift (see §2.6 of the text for codes); (16) Additional notes: A : AT20G source ([Murphy et al. 2010](#)), F : Fermi gamma-ray source (3FGL; [Acero et al. 2015](#)), P : Peaked-spectrum source ([Callingham et al. 2017](#)), ★ : See individual notes in Appendix.

**Table 4.** Expanded list of strongly-scintillating ( $NSI \geq 0.90$ ,  $NormSNR \geq 8.0$ ) sources from the Chhetri et al. (2018a) IPS sample, with no restriction on sky area. This table includes some objects from the main IPS-FIRST sample listed in Table 3 and the IPS-MRC-1Jy sample listed in Table 5 – these are indicated by a  $\diamond$  and a  $\dagger$  respectively in column 14.

GLEAM name	Alt name	$S_{162}$ Jy	$\pm$ Jy	Norm SNR	NSI	NVSS position (J2000)		WISE match	W1 mag	$\pm$	z	z_ref	Notes
(1)	(2)	(3)	(4)	(5)	(6)	RA (7)	Dec (8)	(9)	(10)	(11)	(12)	(13)	(14)
J000905-205630	PKS 0006-212	1.322	0.017	11.5	1.01	00 09 06.02	-20 56 32.3	J000905.98-205632.5	16.166	0.059	0.91	Mc96	P
J001343-253709	PMN J0013-2537	1.319	0.019	10.5	0.93	00 13 44.17	-25 37 12.2	J001344.10-253712.4	16.646	0.088	..	..	
J001821-111139	MRC 0015-114	1.932	0.020	16.2	0.95	00 18 22.04	-11 11 38.2	J001821.92-11139.1	17.042	0.128	..	..	$\diamond$
J001931-043543	3C 007	4.523	0.018	16.4	1.03	00 19 31.49	-04 35 47.8	J001931.48-043548.1	16.573	0.087	..	..	$\diamond$
J002105-184435	NVSS J002105-184438	0.976	0.017	11.1	0.90	00 21 05.96	-18 44 38.0	J002106.00-184438.4	15.819	0.047	..	..	
J002208-104133	PKS 0019-109	1.774	0.019	14.3	1.34	00 22 08.97	-10 41 32.6	J002209.00-104132.1	17.419	0.175	..	..	P $\diamond$
J002223-070230	PKS 0019-073	3.821	0.016	23.1	1.25	00 22 23.04	-07 02 35.1	..	..	..	..	..	$\star$ P $\diamond$
J002546-124724	MRC 0023-130B	1.388	0.021	15.4	1.14	00 25 46.66	-12 47 25.2	J002546.68-124724.9	15.850	0.051	..	..	
J003119-165202	PMN J0031-1651	0.718	0.015	8.5	1.08	00 31 19.07	-16 52 07.7	J003119.14-165208.3	17.312	0.157	..	..	P
J003201-085133	PKS 0029-091	2.125	0.020	16.6	1.27	00 32 00.98	-08 51 37.6	J003200.97-085139.1	17.593	0.212	..	..	P $\diamond$
J003242-123339	PMN J0032-1233	1.132	0.019	11.6	1.16	00 32 42.57	-12 33 39.2	J003242.28-123338.0	15.941	0.056	..	..	$\star$
J003829-211957	PKS 0035-216	1.081	0.017	13.9	1.12	00 38 29.93	-21 20 04.0	J003829.96-212004.0	14.286	0.027	0.338	Mc96	AP $\dagger$
J003931-111057	PMN J0039-1111	1.006	0.019	11.0	1.10	00 39 31.57	-11 11 02.3	J003931.58-111102.6	13.907	0.027	0.5526	SDSS	A
J004106-131440	TXS 0038-135	0.637	0.020	8.4	1.14	00 41 06.43	-13 14 39.7	J004106.42-131438.2	16.116	0.064	..	..	
J004258-203649	PKS 0040-208	1.207	0.016	15.0	0.99	00 42 58.38	-20 37 13.0	J004258.36-203713.2	12.321	0.023	0.6554	6dFGS	$\dagger$
J004537-273534	PMN J0045-2735	0.829	0.015	9.5	1.25	00 45 37.13	-27 35 38.1	J004537.04-273538.8	16.001	0.056	..	..	P
J004807-183838	MRC 0045-189	1.340	0.015	18.0	1.12	00 48 07.55	-18 38 41.6	J004807.64-183840.3	16.836	0.116	..	..	
J004839-294718	PKS 0046-300	1.611	0.015	16.33	1.25	00 48 39.49	-29 47 18.5	..	19.4	0.9	..	..	$\star$ P
J004954-100613	PKS 0047-10	2.257	0.018	27.3	1.05	00 49 54.09	-10 06 14.4	J004954.03-100614.5	16.183	0.061	2.236	SDSS	A $\diamond$
J005026-120115	PKS 0048-12	1.950	0.020	25.5	1.05	00 50 25.94	-12 01 17.0	J005025.57-120110.4	14.814	0.033	..	..	$\star$ A
J005027-175237	TXS 0047-181	0.668	0.016	9.5	1.17	00 50 27.67	-17 52 39.6	..	18.31	0.30	..	..	$\star$
J005039-102734	MRC 0048-107	2.138	0.018	26.8	0.90	00 50 39.04	-10 27 35.2	..	15.67	0.05	..	..	$\star$ $\diamond$
J005234-093819	MRC 0050-099	1.472	0.018	17.2	1.19	00 52 34.53	-09 38 19.2	..	..	..	..	..	$\diamond$
J005315-070232	PMN J0053-0702	1.036	0.016	9.2	0.94	00 53 15.65	-07 02 33.4	J005315.67-070232.5	16.313	0.069	..	..	
J005429-235127	MRC 0052-241	2.818	0.017	38.8	0.92	00 54 29.85	-23 51 31.2	..	..	..	2.86	Mc96	$\dagger$
J005433-195255	PMN J0054-1952	0.726	0.016	10.7	1.06	00 54 32.94	-19 53 00.7	J005432.93-195301.1	15.856	0.051	..	..	A
J005654-201828	NVSS J005653-201834	0.639	0.015	8.7	1.35	00 56 53.97	-20 18 34.3	..	..	..	..	..	
J005930-184204	NVSS J005930-184209	0.572	0.016	9.0	1.24	00 59 30.25	-18 42 09.8	J005930.27-184209.6	14.527	0.03	..	..	
J010021-074718	MRC 0057-080	0.942	0.015	9.9	0.90	01 00 21.01	-07 47 17.8	J010021.14-074718.4	16.771	0.099	..	..	
J010042-050237	MRC 0058-053	1.910	0.016	13.2	1.34	01 00 42.67	-05 02 36.4	J010042.64-050236.5	15.987	0.052	..	..	P $\diamond$
J010152-283118	PKS 0059-287	0.983	0.014	10.0	1.20	01 01 52.38	-28 31 19.7	J010152.37-283120.5	16.020	0.052	1.6	Ka98	AP
J010202-261447	NVSS J010202-261450	0.878	0.016	11.1	1.11	01 02 02.71	-26 14 50.8	J010202.68-261451.3	17.427	0.156	..	..	
J010250-140230	PMN J0102-1402	0.804	0.016	11.95	1.03	01 02 51.10	-14 02 33.2	J010251.06-140233.4	16.702	0.091	..	..	
J010316-322550	PKS 0100-326	3.615	0.012	24.5	0.98	01 03 16.77	-32 25 51.8	J010316.79-322552.3	14.342	0.028	0.256	Dr03	P
J010335-271506	PKS 0101-275	3.077	0.015	36.3	0.99	01 03 35.49	-27 15 11.1	J010335.60-271510.3	17.589	0.178	..	..	P $\dagger$

GLEAM name	Alt name	S <sub>162</sub> Jy	± Jy	Norm SNR	NSI	NVSS position (J2000)		WISE match	W1 mag	±	z	z_ref	Notes
(1)	(2)	(3)	(4)	(5)	(6)	RA	Dec	(9)	(10)	(11)	(12)	(13)	(14)
J010452-252052	PKS 0102-256	3.391	0.016	44.2	1.06	01 04 52.32	-25 20 53.3	J010452.24-252054.5	17.130	0.132	..	..	†
J010527-182843	PKS 0103-187	1.028	0.016	16.0	1.00	01 05 27.04	-18 28 45.7	J010527.05-182846.3	15.175	0.036	..	..	A
J010607-114246	MRC 0103-119	1.511	0.020	20.3	1.18	01 06 7.98	-11 42 46.6	..	..	..	..	..	P
J010617-233615	PMN J0106-2336	0.594	0.018	9.0	1.07	01 06 17.42	-23 36 16.0	J010617.45-233616.9	15.111	0.036	..	..	P
J010703-222257	PMN J0107-2223	0.725	0.015	9.7	1.06	01 07 03.83	-22 23 00.2	J010703.84-222300.8	17.005	0.112	..	..	P
J010837-285124	PKS 0106-291	5.040	0.014	50.0	1.17	01 08 37.88	-28 51 27.7	J010837.89-285129.4	16.916	0.102	..	..	AP †
J010938-144228	MRC 0107-149	2.864	0.020	39.1	0.93	01 09 38.83	-14 42 34.9	J010938.86-144233.9	16.783	0.100	..	..	
J011049-074142	PKS 0108-079	0.723	0.015	9.0	0.94	01 10 50.01	-07 41 41.6	J011050.00-074141.1	15.362	0.039	1.776	Wr83	A
J011156-302623	TXS 0109-307	0.990	0.013	9.2	1.24	01 11 55.97	-30 26 26.2	J011156.00-302622.2	16.019	0.055	..	..	★ P
J011312-101419	PKS 0110-105	1.565	0.019	20.2	1.46	01 13 12.08	-10 14 21.8	J011312.09-101421.2	15.285	0.037	1.3210	SDSS	A
J011651-205202	PKS 0114-21	14.387	0.020	176.6	0.90	01 16 51.43	-20 52 06.6	J011651.48-205207.1	16.363	0.069	1.41	Mc96	AP †
J011657-141105	TXS 0114-144	0.638	0.020	8.3	1.06	01 16 57.88	-14 11 10.5	J011657.86-141110.2	16.178	0.056	..	..	
J011738-150750	PKS 0115-153	0.921	0.021	12.6	1.15	01 17 38.93	-15 07 54.6	J011738.93-150754.8	16.208	0.059	..	..	
J011806-135542	TXS 0115-141	0.806	0.021	9.2	1.43	01 18 06.29	-13 55 48.0	J011806.36-135547.3	17.525	0.148	..	..	P
J011815-012037	PKS 0115-01	5.357	0.020	16.4	1.20	01 18 15.36	-01 20 30.3	J011815.39-012030.2	15.557	0.047	1.162	Ho03	AP ◇
J011823-132620	MRC 0115-137	2.194	0.020	26.6	1.02	01 18 24.17	-13 26 23.9	J011824.19-132624.0	16.273	0.059	..	..	
J011857-071855	MRC 0116-075	1.109	0.017	10.0	1.61	01 18 57.49	-07 18 56.7	J011857.53-071855.6	16.656	0.087	..	..	P
J011915-162313	TXS 0116-166B	1.357	0.019	16.4	0.93	01 19 15.27	-16 23 19.1	J011915.31-162319.2	17.229	0.126	..	..	
J011930-113302	MRC 0117-118	1.266	0.019	15.5	1.13	01 19 30.52	-11 33 07.6	..	..	..	..	..	P
J012102-094426	PMN J0121-0944	0.783	0.020	8.9	1.25	01 21 2.11	-09 44 29.7	J012102.07-094428.6	16.144	0.063	..	..	
J012114-182719	PKS 0118-187	1.074	0.017	14.2	1.16	01 21 14.51	-18 27 22.5	J012114.48-182724.6	17.739	0.202	..	..	P
J013056-150232	PKS 0128-152	2.553	0.019	30.7	0.91	01 30 56.73	-15 02 36.0	J013056.69-150235.6	16.378	0.073	..	..	
J013212-065232	PKS 0129-07	5.309	0.020	36.7	1.19	01 32 12.20	-06 52 36.8	J013212.24-065236.0	15.951	0.051	..	..	AP ◇
J013243-165444	PKS 0130-17	1.453	0.018	14.0	0.92	01 32 43.41	-16 54 47.7	J013243.48-165448.5	12.309	0.025	1.02	Wr83	AFP
J013919-124741	TXS 0136-130	1.029	0.019	8.3	1.16	01 39 19.91	-12 47 42.5	..	18.29	0.32	..	..	★ P
J014013-095654	PKS 0137-10	4.351	0.021	33.5	0.96	01 40 12.82	-09 56 57.1	J014012.84-095657.7	16.327	0.066	..	..	AP ◇
J014045-291744	MRC 0138-295	1.554	0.016	8.3	1.10	01 40 45.82	-29 17 51.2	J014045.87-291750.4	16.300	0.063	..	..	
J014144-074607	MRC 0139-080	1.649	0.018	12.9	1.01	01 41 44.06	-07 46 11.8	J014143.95-074611.4	17.357	0.133	..	..	◇
J015208-192323	MRC 0149-196	1.391	0.015	10.8	1.12	01 52 08.73	-19 23 25.4	J015208.71-192325.2	16.809	0.092	..	..	
J015455-204023	MRC 0152-209	2.471	0.014	15.4	1.14	01 54 55.73	-20 40 26.9	..	16.259	0.036	1.9212	Mc91	★ †

**Table columns:** (1) GLEAM name for the source; (2) Alternative name; (3) 162 MHz flux density in Jy, from [Chhetri et al. \(2018a\)](#); (4) Uncertainty in 162 MHz flux density; (5) Normalised S/N ratio from [Chhetri et al. \(2018a\)](#); (6) Normalised scintillation index, or an upper limit for sources where IPS was not detected; (7) NVSS Right Ascension; (8) NVSS Declination; (9) Name of matched WISE source (if any); (10) WISE W1 magnitude; (11) Uncertainty in W1; (12) Optical spectroscopic redshift (if available); (13) Reference for optical redshift (see §2.6 of the text for codes); (14) Additional notes: A : AT20G source ([Murphy et al. 2010](#)), F : Fermi gamma-ray source (3FGL; [Acero et al. 2015](#)), P : Peaked-spectrum source ([Callingham et al. 2017](#)) , ★ : See individual notes in Appendix, ◇ : Source also included in Table 3 , † : Source also included in Table 5.



**Table 5.** The IPS-MRC-1Jy sample of sources from the Chhetri et al. (2018a) IPS sample that also appear in the MRC-1Jy sample (McCarthy et al. 1996; Kapahi et al. 1998b).

GLEAM name	MRC name	S162 Jy	$\pm$ Jy	Norm SNR	NSI	Radio position (J2000)		T	WISE match	W1 mag	$\pm$	z	z_ref	Notes
(1)	(2)	(3)	(4)	(5)	(6)	RA	Dec	(9)	(10)	(11)	(12)	(13)	(14)	(15)
J000347-232938	MRC 0001-237	3.040	0.021	20.3	< 0.17	00 03 47.89	-23 29 42.1	gal	J000347.92-232941.6	14.398	0.030	0.315	Mc96	
J000402-230657	MRC 0001-233	2.023	0.020	13.9	< 0.44	00 04 02.55	-23 06 57.4	gal	J000402.48-230657.0	13.507	0.025	0.097	Mc96	
J000957-282930	MRC 0007-287	2.212	0.019	14.1	< 0.37	00 09 58.67	-28 29 30.1	gal	J000958.73-282930.0	(12.821)	0.023	..	..	★
J001757-223800	MRC 0015-229	2.385	0.017	22.7	< 0.27	00 17 58.23	-22 38 03.4	gal	J001758.16-223803.2	16.870	0.109	2.01	Mc96	
J002021-202846	MRC 0017-207	1.946	0.019	18.8	< 0.32	00 20 21.49	-20 28 51.4	QSO	J002021.48-202851.0	14.750	0.030	0.545	Ba99	
J002026-201427	MRC 0017-205	2.714	0.020	26.6	< 0.06	00 20 33.18	-20 16 10.5	gal	J002033.23-201611.2	14.392	0.028	0.197	Mc96	
J002308-250232	MRC 0020-253	8.972	0.020	81.7	0.10	00 23 08.90	-25 02 29.1	gal	J002308.86-250229.6	15.564	0.066	0.35	Mc96	
J002430-292847	MRC 0022-297	15.271	0.018	104.7	0.13	00 24 30.14	-29 28 54.6	QSO	J002430.15-292854.3	13.392	0.026	0.4065	Ba99	A
J002448-204259	MRC 0022-209	1.567	0.018	16.2	< 0.16	00 24 47.81	-20 42 39.9	gal	J002447.76-204239.7	13.422	0.025	0.054	Mc96	
J002549-260211	MRC 0023-263	18.786	0.020	153.7	0.78	00 25 49.29	-26 02 12.9	gal	J002549.22-260212.3	14.559	0.031	0.322	Mc96	AP
J002613-200455	MRC 0023-203	5.736	0.017	61.2	0.23	00 26 14.11	-20 04 56.4	gal	J002614.09-200456.1	15.636	0.047	0.845	Mc96	A
J002729-273113	MRC 0025-277	2.676	0.018	23.5	0.32	00 27 29.32	-27 31 12.1	gal	J002729.11-273113.4	17.718	0.199	..	..	
J002752-200738	MRC 0025-204	1.566	0.017	17.4	0.40	00 27 52.80	-20 07 38.4	gal	J002752.86-200738.7	15.472	0.042	..	..	
J003102-220701	MRC 0028-223	1.745	0.015	21.0	< 0.23	00 31 02.46	-20 07 08.3	gal	J003102.44-220708.3	14.082	0.027	0.205	Mc96	
J003150-265223	MRC 0029-271	2.282	0.017	21.8	0.57	00 31 50.4	-26 52 25	QSO	J003150.49-265224.6	13.869	0.025	0.333	Ba99	
J003203-225759	MRC 0029-232	2.554	0.017	29.2	0.27	00 32 03.60	-22 58 08.6	gal	J003203.30-225804.1	16.772	0.090	..	..	
J003221-240505	MRC 0029-243	3.973	0.018	49.2	0.39	00 32 21.33	-24 05 09.1	gal	J003221.32-240507.8	16.118	0.057	1.29	Mc96	
J003244-214414	MRC 0030-220	1.785	0.016	21.3	0.29	00 32 44.7	-21 44 22	QSO	J003244.71-214421.9	15.612	0.049	0.806	Ba99	
J003246-293107	MRC 0030-297	2.632	0.016	21.2	0.71	00 32 46.26	-29 31 10.0	gal	J003246.22-293110.7	16.529	0.077	..	..	P
J003323-214154	MRC 0030-219	1.686	0.016	20.1	0.86	00 33 23.88	-21 42 00.4	gal	J003323.85-214201.7	17.538	0.191	2.168	Mc96	
J003508-200354	MRC 0032-203	12.487	0.017	160.8	0.47	00 35 09.21	-20 03 55.3	gal	J003508.79-200359.4	14.096	0.027	0.516	Mc96	A
J003722-230825	MRC 0034-234	3.563	0.017	43.9	0.14	00 37 22.14	-23 08 30.2	gal	J003722.27-230831.0	16.161	0.060	..	..	
J003824-225256	MRC 0035-231	2.327	0.016	29.7	0.46	00 38 24.82	-22 53 02.6	gal	J003824.93-225302.5	15.470	0.043	0.685	Mc96	
J003829-211957	MRC 0036-216	1.081	0.017	13.9	1.12	00 38 30.03	-21 20 04.7	gal	J003829.96-212004.0	14.286	0.027	0.338	Mc96	AP
J003956-253425	MRC 0037-258	2.591	0.016	31.2	< 0.22	00 39 56.40	-25 34 30.0	gal	J003956.45-253431.0	15.902	0.052	1.1	Mc96	
J004048-204329	MRC 0038-209	1.710	0.017	21.2	0.39	00 40 48.13	-20 43 39.9	gal	J004048.20-204339.6	12.775	0.024	0.0906	Mc96	A
J004112-290744	MRC 0038-294	1.967	0.016	21.1	< 0.29	00 41 12.14	-29 07 46.9	gal	J004111.62-290748.3	16.460	0.064	..	..	
J004258-203649	MRC 0040-208	1.207	0.016	15.0	0.99	00 42 58.4	-20 37 14	QSO	J004258.36-203713.2	12.321	0.023	0.6554	Ba99	
J004411-221219	MRC 0041-224	3.935	0.016	53.8	0.31	00 44 11.98	-22 12 18.3	gal	..	..	..	..	..	
J004503-243417	MRC 0042-248	2.644	0.017	33.5	< 0.18	00 45 03.12	-24 34 23.6	gal	J004502.95-243423.8	14.635	0.031	..	..	
J004733-251710	MRC 0045-255	6.577	0.020	66.7	0.07	00 47 27.41	-25 13 37.9	gal	J004733.14-251717.7	5.757	0.034	0.001	RC3	AF
J005053-230650	MRC 0048-233	1.854	0.016	25.5	< 0.20	00 50 53.04	-23 06 53.8	gal	J005052.87-230654.1	13.287	0.046	0.111	Mc96	
J005242-215540	MRC 0050-222	2.454	0.016	34.1	0.85	00 52 42.79	-21 55 45.2	gal	J005242.84-215546.7	15.635	0.045	0.654	Mc96	
J005429-235127	MRC 0052-241	2.818	0.017	38.8	0.92	00 54 29.82	-23 51 29.7	gal	..	..	..	2.86	Mc96	
J005742-253313	MRC 0055-258	1.049	0.017	12.8	< 0.30	00 57 42.64	-25 33 14.4	gal	J005742.75-253315.6	15.054	0.038	..	..	

GLEAM name	MRC name	S162 Jy	$\pm$ Jy	Norm SNR	NSI	Radio position (J2000)		T	WISE match	W1 mag	$\pm$	z	z_ref	Notes
(1)	(2)	(3)	(4)	(5)	(6)	RA	Dec	(9)	(10)	(11)	(12)	(13)	(14)	(15)
J005756-252233	MRC 0055-256	1.301	0.017	16.6	< 0.35	00 57 57.05	-25 22 36.7	gal	J005756.98-252237.4	14.135	0.027	0.1985	Mc96	
J005827-240101	MRC 0056-242	3.676	0.016	53.0	< 0.11	00 58 27.79	-24 01 05.4	gal	J005827.81-240104.8	14.727	0.030	..	..	
J010041-223955	MRC 0058-229	2.605	0.016	36.0	< 0.15	01 00 42.0	-22 39 58	QSO	J010042.10-223959.8	14.165	0.027	0.706	Ba99	
J010241-215227	MRC 0100-221	9.191	0.018	114.4	0.04	01 02 41.69	-21 52 53.8	gal	J010241.76-215254.2	11.451	0.022	0.058	Mc96	
J010244-273124	MRC 0100-277	5.929	0.015	68.4	0.20	01 02 43.92	-27 31 24.8	gal	J010244.00-273126.0	15.540	0.041	..	..	
J010335-271506	MRC 0101-275	3.077	0.015	36.3	0.99	01 03 35.48	-27 15 09.2	gal	J010335.60-271510.3	17.589	0.178	..	..	P
J010452-252052	MRC 0102-256	3.391	0.016	44.2	1.06	01 04 52.17	-25 20 53.1	gal	J010452.24-252054.5	17.130	0.132	..	..	
J010612-240634	MRC 0103-243	2.076	0.017	27.5	0.22	01 06 12.61	-24 06 38.4	gal	J010612.70-240635.5	17.014	0.104	..	..	
J010837-285124	MRC 0106-291	5.040	0.014	50.0	1.17	01 08 37.98	-28 51 28.6	gal	J010837.89-285129.4	16.916	0.102	..	..	AP
J010902-230728	MRC 0106-233	1.937	0.015	26.9	0.63	01 09 03.0	-23 07 29	QSO	J010903.02-230729.7	14.920	0.035	0.818	Ba99	
J011228-221045	MRC 0110-224	2.390	0.015	32.6	0.55	01 12 28.92	-22 10 49.1	gal	J011228.95-221051.0	15.846	0.052	..	..	
J011342-252358	MRC 0111-256	1.606	0.016	19.9	< 0.29	01 13 42.6	-25 23 59	QSO	J011342.59-252359.0	15.843	0.047	1.05	Ba99	A
J011442-204239	MRC 0112-209	4.638	0.017	59.9	0.28	01 14 42.36	-20 42 49.7	gal	J011442.22-204249.0	16.307	0.069	..	..	
J011516-213834	MRC 0112-219	1.786	0.016	21.6	< 0.19	01 15 16.72	-21 38 37.5	gal	J011516.99-213843.1	15.451	0.041	..	..	
J011539-281707	MRC 0113-285	2.950	0.015	30.6	< 0.27	01 15 39.52	-28 17 07.2	gal	J011539.54-281709.5	15.788	0.044	..	..	A
J011544-241719	MRC 0113-245	2.499	0.016	29.7	0.34	01 15 44.61	-24 17 14.1	gal	J011544.66-241715.0	15.331	0.039	..	..	
J011651-205202	MRC 0114-211	14.387	0.020	176.6	0.90	01 16 51.44	-20 52 07.5	gal	J011651.48-205207.1	16.363	0.069	1.41:	Mc96	AP
J011815-255148	MRC 0115-261	4.329	0.016	48.6	< 0.15	01 18 15.66	-25 51 49.4	gal	J011815.76-255149.6	14.629	0.029	0.268	Mc96	A
J012031-270125	MRC 0118-272	1.866	0.016	20.1	0.51	01 20 31.6	-27 01 25	QSO	J012031.66-270124.6	11.316	0.022	..	..	AF
J012331-291629	MRC 0121-295	2.725	0.015	21.4	< 0.28	01 23 31.50	-29 16 29.6	gal	J012331.51-291630.7	15.421	0.041	..	..	
J012445-251714	MRC 0122-255	6.909	0.016	77.5	0.39	01 24 46.28	-25 17 13.6	gal	J012446.45-251716.9	9.852	0.024	..	..	
J012614-222227	MRC 0123-226	2.567	0.016	29.3	0.29	01 26 15.0	-22 22 34	QSO	J012614.99-222233.6	13.877	0.026	0.72	Ba99	AF
J012730-195607	MRC 0125-201	1.878	0.016	20.4	0.63	01 27 30.66	-19 56 10.4	gal	..	..	..	..	..	..
J012808-212207	MRC 0125-216	1.975	0.014	22.1	< 0.17	01 28 08.73	-21 22 10.9	gal	J012808.59-212211.2	14.179	0.029	0.34	Mc96	
J013009-272440	MRC 0127-276	1.618	0.017	14.7	< 0.53	01 30 09.29	-27 24 41.4	gal	J013008.96-272441.9	15.504	0.046	0.318	Mc96	
J013027-260956	MRC 0128-264	11.522	0.017	102.2	0.35	01 30 27.81	-26 09 55.8	gal	..	..	..	2.348	Be99	
J013525-262333	MRC 0133-266	2.268	0.017	19.4	< 0.16	01 35 25.8	-26 23 32	QSO	J013525.77-262337.7	15.187	0.035	1.53	Ba99	
J013600-272742	MRC 0133-277	2.266	0.016	17.3	< 0.03	01 36 00.45	-27 27 44.3	gal	J013600.50-272744.3	16.335	0.071	..	..	
J013737-243048	MRC 0135-247	3.760	0.016	35.9	0.27	01 37 38.3	-24 30 54	QSO	J013738.34-243053.9	12.920	0.024	0.8375	Ba99	AF
J013857-225444	MRC 0136-231	2.468	0.016	23.6	< 0.28	01 38 57.4	-22 54 47	QSO	J013857.46-225447.3	14.892	0.032	1.893	Ba99	A
J013952-260648	MRC 0137-263	2.772	0.016	20.7	< 0.29	01 39 52.60	-26 07 06.3	gal	J013952.63-260710.1	16.688	0.074	..	..	
J014112-213825	MRC 0138-218	1.662	0.015	15.0	< 0.39	01 41 12.29	-21 38 32.7	gal	J014112.18-213841.6	15.840	0.054	..	..	
J014127-270606	MRC 0139-273	8.202	0.017	57.5	0.65	01 41 27.08	-27 06 11.4	gal	J014127.03-270611.6	16.187	0.056	1.44	Mc96	A
J014241-253033	MRC 0140-257	2.148	0.016	14.7	0.58	01 42 41.16	-25 30 34.1	gal	J014241.25-253036.5	17.615	0.151	2.64	Mc96	
J014521-242333	MRC 0143-246	3.123	0.018	24.9	0.33	01 45 21.30	-24 23 35.0	gal	J014521.34-242331.0	15.314	0.039	0.716	Mc96	

GLEAM name	MRC name	S162 Jy	$\pm$ Jy	Norm SNR	NSI	Radio position (J2000)		T	WISE match	W1 mag	$\pm$	z	z_ref	Notes
(1)	(2)	(3)	(4)	(5)	(6)	(7)	(8)	(9)	(10)	(11)	(12)	(13)	(14)	(15)
J014709-223234	MRC 0144-227	1.977	0.015	16.8	0.81	01 47 09.26	-22 32 42.0	gal	J014709.23-223241.0	15.733	0.045	0.6	Mc96	
J014913-221129	MRC 0146-224	2.326	0.016	16.3	< 0.26	01 49 13.94	-22 11 37.8	gal	J014913.99-221137.0	14.748	0.034	0.36	Mc96	
J015035-293158	MRC 0148-297	11.405	0.019	43.6	< 0.11	01 50 35.86	-29 31 56.0	gal	J015035.94-293155.3	14.636	0.029	0.41	Mc96	
J015223-271855	MRC 0150-275	3.659	0.017	18.0	0.44	01 52 23.49	-27 18 55.7	gal	J015223.54-271856.6	15.788	0.045	..	..	
J015455-204023	MRC 0152-209	2.471	0.014	15.4	1.14	01 54 55.72	-20 40 26.8	gal	(uncataloged)	16.259	0.036	1.9212	Mc91	★
J015753-210216	MRC 0155-212	3.865	0.014	20.7	< 0.31	01 57 53.26	-21 02 19.3	gal	J015753.40-210217.0	13.101	0.023	0.159	Mc96	
J015814-222036	MRC 0155-225	2.635	0.015	13.0	< 0.43	01 58 14.45	-22 20 42.1	gal	J015814.58-222044.7	15.680	0.045	..	..	
J015833-245928	MRC 0156-252	3.018	0.016	13.6	0.67	01 58 33.45	-24 59 30.2	gal	J015833.45-245931.9	15.401	0.038	2.09	Mc96	
J234324-214129	MRC 2340-219	4.525	0.012	14.9	< 0.18	23 43 24.21	-21 41 33.8	gal	J234324.28-214135.3	15.097	0.036	0.766	Mc96	
J234545-240232	MRC 2343-243	3.663	0.014	13.3	< 0.57	23 45 45.17	-24 02 31.2	gal	J234545.18-240231.0	14.044	0.027	0.6	Mc96	A
J235050-245702	MRC 2348-252	9.403	0.015	39.3	< 0.19	23 50 49.7	-24 57 03	QSO	J235049.80-245703.5	14.159	0.029	1.39	Ba99	
J235128-231708	MRC 2348-235	2.826	0.014	12.6	< 0.39	23 51 28.27	-23 17 05.8	gal	J235128.27-231706.3	16.041	0.057	0.952	Mc96	
J235352-231126	MRC 2351-234	2.913	0.014	14.9	< 0.45	23 53 52.25	-23 11 29.0	gal	J235352.35-231127.9	15.275	0.038	1.03	Mc96	
J235410-215647	MRC 2351-222	2.656	0.013	14.0	< 0.43	23 54 10.55	-21 56 50.7	gal	J235410.61-215651.7	15.952	0.061	..	..	
J235735-211319	MRC 2355-214	3.321	0.013	23.4	0.73	23 57 35.27	-21 13 27.6	gal	J235735.42-211322.5	16.398	0.072	1.41	Mc96	P

**Table columns:** (1) GLEAM name for the source; (2) Alternative name; (3) 162 MHz flux density in Jy, from [Chhetri et al. \(2018a\)](#); (4) Uncertainty in 162 MHz flux density; (5) Normalised S/N ratio from [Chhetri et al. \(2018a\)](#); (6) Normalised scintillation index, or an upper limit for sources where IPS was not detected; (7,8) Radio position from the MRC-1Jy catalogue; (9) Type (galaxy or QSO); (10) Name of matched WISE source (if any); (11) WISE W1 magnitude; (12) Uncertainty in W1; (13) Optical spectroscopic redshift (if available); (14) Reference for optical redshift (see §2.6 of the text for codes); (15) Additional notes: A : AT20G source ([Murphy et al. 2010](#)), F : Fermi gamma-ray source (3FGL; [Acero et al. 2015](#)), P : Peaked-spectrum source ([Callingham et al. 2017](#)), ★ : See individual notes in Appendix.

**APPENDIX A: NOTES ON INDIVIDUAL SOURCES****GLEAM J000958.73-282930.0** (MRC 0007-287)

McCarthy et al. (1996) note that this source is occulted by a bright star. As a result, the catalogued W1 magnitude is unreliable and no redshift has yet been measured for the host galaxy.

**GLEAM J001356-091952** (PKS 0011-096)

An SDSS spectrum shows strong, narrow optical emission lines, including high-excitation lines of [Ne III] and [Ne V].

**GLEAM J002223-070230** (PKS 0019-073)

The host of this radio source remains unidentified. The closest WISE source is 10 arcsec from the FIRST radio position, and is unlikely to be associated.

**GLEAM J003242-123339** (PMN J0032-1233)

Based on a visual inspection of the WISE images, we identify the WISE object WISE J003242.28-123338.0 as the host of this compact radio source. Although the WISE object is offset by 4.3 arcsec from the NVSS radio position (which itself has a 1.5 arcsec uncertainty), its W1-W2 colour of 0.84 mag. implies that it is a powerful AGN and so is unlikely to be a chance alignment of a foreground galaxy.

**GLEAM J003251-101801** (MRC 0030-105)

This is a compact (angular separation  $\sim 10$  arcsec) double source in FIRST, with a well-defined radio centroid. The closest WISE source is 6.6 arcsec from the radio centroid and appears to be unrelated. The host of this radio source therefore remains unidentified.

**GLEAM J003931-111057** (PMN J0039-1111)

An SDSS spectrum shows strong optical emission lines, including high-excitation lines of [Ne III], along with a strong, broad Mg II emission line.

**GLEAM J004049-094832** (MRC 0038-100)

There is no catalogued WISE source within 15-20 arcsec of the radio centroid of this double source, and the host of this source remains unidentified.

**GLEAM J004246-061325** (PKS 0040-06)

This GLEAM source corresponds to the northern hotspot of a wide double with a total angular extent of the radio source of at least 6 arcmin. The radio position listed by van Velzen et al. (2015) for this source (J2000: 00 42 45.77 -06 12 41.3) also corresponds to the northern hotspot rather than the whole source. The correct optical identification (with a 17th magnitude galaxy) was first made by Bolton et al. (1971). The position listed in columns 9 and 10 of Table 3 is that of the optical galaxy, rather than the FIRST radio centroid. The SDSS spectrum shows narrow optical emission lines superimposed on a stellar continuum. At the SDSS redshift of  $z=0.1243$ , the projected linear size of the source is over 800 kpc.

**GLEAM J004839-2947189** (PKS 0046-300)

A faint uncatalogued source is visible in the WISE W1 image, at an offset of 2.5 arcsec from the NVSS radio

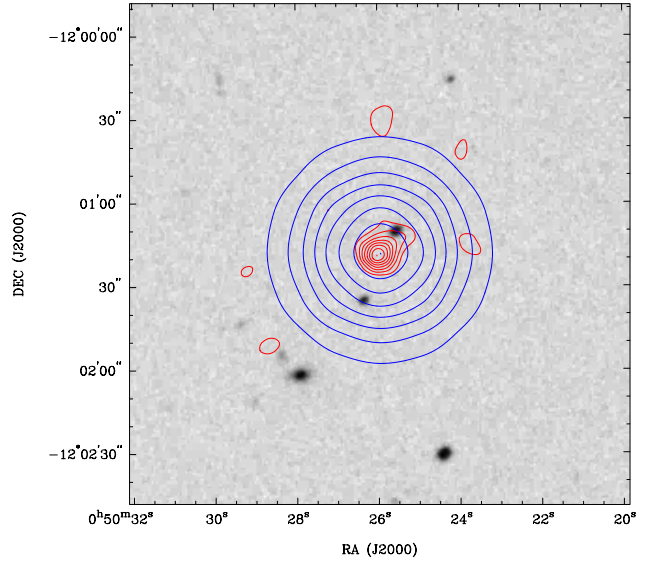


**Figure A1.** Radio contours from the AT20G survey at 20 GHz (red) and the NVSS survey at 1.4 GHz (blue) overlaid on an optical image of the field of PKS 0048-12 (GLEAM J005026-120115). The 20 GHz contours are elongated towards a bright, unresolved optical/IR object, WISE J0005025.57-120110.4, which has optical and mid-IR colours characteristic of a QSO.

position. One of us (THJ) measured a magnitude of  $W1 = 19.4 \pm 0.9$  mag. for this object, which we tentatively identify as the host of the radio source. This WISE source was not detected in the W2-W4 bands.

**GLEAM J005026-120115** (PKS 0048-12)

A bright WISE source located 7 arcsec from the radio centroid has mid-IR colours typical of QSO, and is also detected as a ROSAT X-ray source. Based on the radio morphology seen in the higher-resolution AT20G image, where the radio contours are extended in the direction of the optical object (see Figure A1), it appears probable that the strongly-scintillating low-frequency source is one hotspot of a radio-loud QSO. We therefore identify this WISE source as the likely host of the radio source PKS 0048-12.

**GLEAM J005027-175237** (TXS 0047-181)

There is a faint, uncatalogued WISE source (with  $W1 = 18.31 \pm 0.30$  mag, and undetected in the W2-W4 bands) offset by 6.1 arcsec from the NVSS radio position. It is unclear at this stage whether this faint object is associated with the radio source. The WISE image shows other faint sources nearby, suggesting the possible presence of a distant cluster of galaxies.

**GLEAM J005039-102734** (MRC 0048-107)

A visual inspection of the WISE W1 image shows two mid-IR sources close to the FIRST radio position. The closest object listed in the WISE catalogue (WISE J005038.95-102739.4 with  $W1 = 15.78$  mag) is 3.0 arcsec away, but a second uncatalogued object is closer to the FIRST radio centroid. Based on measurements of the WISE made by one of us (THJ), we adopt WISE values of  $W1 = 15.67 \pm 0.05$ ,  $W2 = 15.21 \pm 0.14$  and  $W3 = 10.2 \pm 0.95$  mag. for the

radio-source host (which is not detected in the W4 band).

**GLEAM J005536-095216** (MRC 0053-101)

The host of this double source remains unidentified, though there is a faint uncatalogued WISE object close to the radio centroid that appears more prominent in W2 than in the W1 band. The closest catalogued WISE source (with  $W1 = 15.06 \pm 0.04$  mag) is 5.3 arcsec away and is unlikely to be associated.

**GLEAM J005734-012329** (3C 29)

This GLEAM source is associated with the nearby galaxy UGC 595, and is resolved into a pair of double sources in FIRST. The radio position listed in columns 9 and 10 of Table 3 is that of the 20 GHz core source detected in the AT20G survey (Murphy et al. 2010), rather than the FIRST radio centroid.

**GLEAM J010159-105555** (TN J0102-07)

De Breuck et al. (2002) obtained deep K-band imaging of the host of this ultra steep-spectrum radio source, and identified it with a faint ( $K \sim 19$  mag) galaxy. There is no catalogued WISE source near the FIRST radio position, implying that the host is fainter than about 17.2 mag in the WISE W1 band (as expected from the De Breuck et al. (2002) imaging result).

**GLEAM J011156-302623** (TXS 0109-307)

We tentatively identify this radio source with a WISE object located 3.9 arcsec from the catalogued NVSS position.

**GLEAM J011406-100800** (PMN J0114-1007)

A faint WISE source, WISE J011406.33-100802.6 with  $W1 = 16.80$  mag, is located 3.7 arcsec from the FIRST radio position. Given the extended nature of the FIRST source (which makes the position of the radio centroid less certain), and the AGN-like colours of the WISE source ( $W1-W2 = 0.74$  mag), we adopt the WISE object as the correct radio-source host.

**GLEAM J011645-041849** (MRC 0114-045)

An SDSS spectrum shows strong emission lines, including high-excitation [Ne III] and [Ne V] lines as well as broad Balmer emission lines.

**GLEAM J012227-042123** (PKS 0119-04)

An SDSS spectrum is available for this radio-loud QSO (SDSS J012227.89-042127.1), with the SDSS redshift listed as  $z = 2.7838$ . This is inconsistent with the value of  $z = 1.925$  published by Osmer et al. (1994) and is also inconsistent with the position of several of the emission lines seen in the SDSS spectrum. The listed SDSS redshift appears to be incorrect, and we therefore adopt the Osmer et al. (1994) redshift of  $z = 1.925$  in this paper.

**GLEAM J012231-061953** (MRC 0120-065)

We tentatively identify this triple FIRST source with a bright WISE objects located near the stronger (eastern) hotspot. Higher-resolution radio images (ideally at frequencies above 5 GHz) would be useful to check this identification.

**GLEAM J012603-012356** (NGC 547)

This GLEAM source corresponds to the southern hotspot of the nearby extended radio galaxy NGC 547 (O’Dea & Owen 1985). The position listed in columns 9 and 10 of Table 3 is that of the optical galaxy, rather than the FIRST radio centroid.

**GLEAM J013136-070354** (PKS 0129-073)

The WISE W1 image shows a faint source near the radio centroid, but the closest catalogued WISE source (WISE J013136.64-070400.4 with  $W1 = 14.41$  mag) is 4.2 arcsec away and appears unlikely to be a radio match.

**GLEAM J013919-124741** (TXS 0136-130)

A faint uncatalogued WISE source is visible near the NVSS radio position. One of us (THJ) has measured the WISE magnitudes of this source as  $W1 = 18.29 \pm 0.32$  mag and  $W2 = 17.26 \pm 0.69$  mag.

**GLEAM J014237-074232** (PKS 0140-07)

There is another (apparently unrelated) radio source about 2 arcmin from the FIRST position, which may confuse the GLEAM image. No nearby counterpart is seen in the WISE W1 image, but a faint optical object (SDSS J014236.44-074303.5) may correspond to the host galaxy.

**GLEAM J015455-204023** (MRC 0152-209)

This  $z=1.92$  radio galaxy (‘the Dragonfly’) is described by Emonts et al. (2015) as “the most infrared-luminous high-redshift radio galaxy known in the southern hemisphere”, and is embedded within a large reservoir of molecular gas (Emonts et al. 2016).

The host galaxy of this source is not listed in the WISE catalogue, probably because it is blended with a nearby star. An object close to the radio position is visible in the WISE image, and one of us (THJ) has measured the following deblended magnitudes for the WISE galaxy:  $W1 = 16.259 \pm 0.036$  mag;  $W2 = 15.177 \pm 0.014$  mag;  $W3 = 11.973 \pm 0.096$  mag;  $W4 = 8.828 \pm 0.081$  mag.

This paper has been typeset from a  $\text{\TeX}/\text{\LaTeX}$  file prepared by the author.